DEUTSCHES ELEKTRONEN – SYNCHROTRON

DESY 91-098
HLRZ 91-71
FUB-HEP/91-9
September 1991

Scaling Laws, Renormalization Group Flow and the Continuum Limit in Non-Compact Lattice QED

M. Göckeler, R. Horsley
Institut für Theoretische Physik, RWTH Aachen
and
Höchstleistungsrechenzentrum HLRZ, c/o KFA Jülich

P. Rakow
Inst. für Theoretische Physik, Freie Universität Berlin

G. Schierholz
Höchstleistungsrechenzentrum HLRZ, c/o KFA Jülich
and
Deutsches Elektronen-Synchrotron DESY, Hamburg

R. Sommer
CERN, Geneva

ISSN 0418-9833

NOTKESTRASSE 85 · D-2000 HAMBURG 52

To be sure that your preprints are promptly included in the
HIGH ENERGY PHYSICS INDEX,
send them to the following (if possible by air mail):

DESY
Bibliothek
Notkestrasse 85
D–2000 Hamburg 52
Germany

DESY 91-098
HLRZ 91-71
FUB-HEP/91-9
September 1991

ISSN 0418-9833

Scaling Laws, Renormalization Group Flow and the Continuum Limit in Non-Compact Lattice QED

M. Göckeler[1,2], R. Horsley[1,2], P. Rakow[3],

G. Schierholz[2,4] and R. Sommer[5]

[1] Institut für Theoretische Physik, RWTH Aachen,

Sommerfeldstraße, D-5100 Aachen, Germany

[2]Gruppe Theorie der Elementarteilchen,

Höchstleistungsrechenzentrum HLRZ,

c/o KFA, Postfach 1913, D-5170 Jülich, Germany

[3] Institut für Theoretische Physik, Freie Universität Berlin,

Arnimallee 14, D-1000 Berlin, Germany

[4] Deutsches Elektronen-Synchrotron DESY,

Notkestraße 85, D-2000 Hamburg 52, Germany

[5] CERN, CH-1211 Geneva 23, Switzerland

Abstract

We investigate the ultra-violet behavior of non-compact lattice QED with light staggered fermions. The main question is whether QED is a non-trivial theory in the continuum limit, and if not, what is its range of validity as a low-energy theory. Perhaps the limited range of validity could offer an explanation of why the fine-structure constant is so small. Non-compact QED undergoes a second order chiral phase transition at strong coupling, at which the continuum limit can be taken. We examine the phase diagram and the critical behavior of the theory in detail. Moreover, we address the question as to whether QED confines in the chirally broken phase. This is done by investigating the potential between static external charges. We then compute the renormalized charge and derive the Callan-Symanzik β function in the critical region. No ultra-violet stable zero is found. Instead, we find that the evolution of charge is well described by renormalized perturbation theory, and that the renormalized charge vanishes at the critical point. The consequence is that QED can only be regarded as a cut-off theory. We evaluate the maximum value of the cut-off as a function of the renormalized charge. Next, we compute the masses of fermion-antifermion composite states. The scaling behavior of these masses is well described by an effective action with mean field critical exponents plus logarithmic corrections. This indicates that also the matter sector of the theory is non-interacting. Finally, we investigate and compare the renormalization group flow of different quantities. Altogether, we find that QED is a valid theory only for small renormalized charges.

1 Introduction

There is considerable interest in the non-perturbative investigation of QED. In particular the ultra-violet behavior of QED has become an important issue. Recent progress in lattice gauge theory, especially in the field of simulating fermions, has made it possible to attack this problem from first principles. In this work we shall present an extensive investigation of non-compact, lattice regularized QED in the vicinity of its critical point. Preliminary results of this work have been reported in refs. [1,2].

QED is the best tested of all field theories. It describes the static properties of electrons and muons to a remarkable precision. But all this success is in the context of perturbation theory, while it is well known that the perturbation series is at most asymptotic. Until very recently not much was known about the ultra-violet behavior, in spite of great calculational efforts [3]. The main obstacle was that the effective charge grows with increasing energy, so that perturbation theory cannot be applied.

The prejudice is that QED, together with all other non-asymptotically free theories, is trivial, in the sense that the renormalized charge vanishes as the cut-off is sent to infinity [4]. We call this limit the continuum limit. If true, QED can only be regarded as a cut-off theory. The maximum value of the cut-off is determined by the magnitude of the renormalized charge. A cut-off theory may be a useful low-energy theory, if the cut-off can be pushed to reasonably large values without changing the low-energy physics. Later on we shall call a theory, which has this property, weakly renormalizable. At the latest at the maximum value of the cut-off new physics is expected to show up, which makes the cut-off behavior of the theory an interesting subject to investigate. In pure QED this value is expected to lie far above the Planck mass, where QED should not be considered in isolation anymore. So, the problem was regarded to be of academic importance only. In the standard model with its many charged particles, and even more so in current composite and supersymmetric models, the cut-off may, however, lie not far from the Planck mass. In this case a close inspection of the ultra-violet behavior might give us a clue of what lies beyond the standard model.

Non-perturbative phenomena of non-asymptotically free (gauge) theories play also a central role in current models of electroweak symmetry breaking. The possible existence of a critical point with large anomalous dimensions has led to a revival of technicolor models [5] and inspired the construction of dynamical Higgs models based on the top quark condensate [6]. QED contains the basic dynamical

structure of such theories. Thus, it provides a useful laboratory for the study of dynamical symmetry breaking in these theories.

The interest in non-perturbative studies of QED began after Miransky [7] investigated a truncated Schwinger-Dyson equation for the fermion propagator and found a continuous chiral phase transition, with chiral symmetry being broken spontaneously at strong coupling. Though his equation did not include any vacuum polarization effects, he argued that the critical coupling should be regarded as an ultra-violet stable fixed point, at which the theory admits a non-trivial continuum limit. The existence of a chiral phase transition was confirmed by numerical studies of non-compact lattice QED in the quenched approximation and with a small number of dynamical fermions [8]. These early lattice investigations also claimed to find support for non-trivial critical behavior. The picture changed when further studies [1,9,10] found critical exponents, which were consistent with mean field theory. Studies of a coupled set of Schwinger-Dyson equations, which include certain effects of fermion loops [11,12], found also mean field critical exponents. Recently, this investigation has been completed by computing the flow of the renormalized charge in the vicinity of the critical point,[1] both on the lattice [2] and from Schwinger-Dyson equations [12,14]. It turned out that the renormalized charge vanishes in the continuum limit, suggesting that the theory is indeed trivial. Evidence for the non-renormalizability of QED was also seen.

The outline of the paper is as follows. Section 2 deals with the technical aspects of the calculation. In sect. 3 we discuss the phase diagram and determine the critical coupling. We find a first order critical line at strong coupling ending in a tricritical point. On this line chiral symmetry is broken spontaneously. We furthermore show that the critical behavior is consistent with mean field theory. For our further analysis it is important to know, whether the vacuum of the chirally broken phase is confining or Coulomb-like. We therefore study the potential between static external test charges in sect. 4. The answer is that there is no sign of confinement. In sect. 5 we compute the renormalized fermion mass from the fermion propagator. For this one needs to fix the gauge. We have chosen the Landau gauge. In appendix A it is shown that the mass does not depend on the choice of covariant gauge, and in appendix B an alternative method of calculating the fermion mass is presented. A serious problem is the occurrence of slowly moving background fields, which have to be treated with special care. The effect of background fields in perturbative calculations on a finite lattice is discussed in appendix C. Finally, we compare the renormalized fermion mass with the chiral

[1] Outside the critical region the renormalization group flow may be computed by means of large mass and perturbative expansions [13].

condensate, in order to shed some light on the mechanism of chiral symmetry breaking. The renormalized charge is computed in sect. 6. This proceeds via the photon propagator in momentum space. Here, the problem is to extrapolate the propagator to zero momentum. We use various methods, which give consistent results. We use these results to compute the potential between static charges to one loop order and find quantitative agreement with the data presented in sect. 4. In sect. 7 we compute the Callan-Symanzik β function and determine the lines of constant renormalized charge. These lines end on the first order critical line, except for the zero charge line, which runs into the critical point. We evaluate the maximum value of the cut-off as a function of the renormalized charge. The masses of fermion-antifermion composite states are computed in sect. 8. Furthermore, their critical behavior is interpreted in terms of an effective action. In sect. 9 we investigate to what extent QED can be regarded as a useful low-energy theory. This requires the existence of lines of constant physics, which can be found by comparing the flow of different dimensionless quantities. In addition to the lines of constant renormalized charge, we compute lines of constant mass ratios, involving the renormalized fermion mass and various masses of fermion-antifermion composite states. Does decoupling of the photon imply triviality of the matter sector also? In sect. 10 we re-examine the critical exponents and relate them to the anomalous dimension of the mass operator. Finally, sect. 11 lists our conclusions.

The reader, who is mainly interested in the results rather than in the details of the calculation, is advised to read the end of sect. 5, sects. 7, 8 and 9 and the conclusions in sect. 11.

2 Lattice calculation

The non-compact formulation of lattice QED shares all the essential features of the continuum theory [15]. It has the property that the photon field interacts only with fermions, whereas the compact theory has monopoles and gives rise to photon-photon interactions. The compact formulation, furthermore, might belong to a different universality class. According to [16,17] it leads to a first order chiral phase transition at strong coupling and therefore admits no continuum limit associated with this transition.[2]

[2]For the mixed gauge field action with large negative adjoint coupling see, however, ref. [18].

The non-compact gauge field action is given by

$$S_G = \frac{\beta}{2} \sum_{x,\mu<\nu} F_{\mu\nu}^2(x) \tag{2.1}$$

with

$$F_{\mu\nu}(x) = \Delta_\mu A_\nu(x) - \Delta_\nu A_\mu(x), \tag{2.2}$$

where Δ_μ is the forward lattice derivative, $\beta = 1/e^2$, and e is the bare charge. In eqs. (2.1) and (2.2) and in the following the lattice constant has been set equal to one for convenience, so that all dimensionful quantities are to be understood in units of the (inverse) lattice spacing. The gauge fields take values on the real line. As long as one only considers gauge invariant quantities, the functional integral can always be made well-behaved, in spite of the unbounded range of integration.

Since chiral symmetry plays a major role in this work, a natural choice for the fermionic variables are staggered fermions. The corresponding action is given by

$$S_F = \sum_{x,y} \bar{\chi}(x)[M_{xy} + m\delta_{xy}]\chi(y), \tag{2.3}$$

$$M_{xy} = \frac{1}{2} \sum_{\mu} (-1)^{x_1+\ldots+x_{\mu-1}} [e^{iA_\mu(x)}\delta_{y\,x+\hat{\mu}} - e^{-iA_\mu(y)}\delta_{y\,x-\hat{\mu}}], \tag{2.4}$$

where m is the bare mass. In the naive continuum limit this action describes four Dirac fermions (flavors) minimally coupled to a $U(1)$ gauge field. For finite lattice spacing it has a chiral $U(1) \times U(1)$ symmetry at $m = 0$, while the $SU(4) \times SU(4)$ symmetry is only approximate. This symmetry is restored in the naive continuum limit. The question of flavor symmetry restoration will be addressed at various stages of the discussion.

Wilson fermions, on the other hand, have no continuous chiral symmetry. In QCD the effect of the Wilson term vanishes in the continuum limit due to asymptotic freedom. In QED this is not so clear, and it is possible that the Wilson action falls into a different universality class from the continuum action.

The calculations in this paper are based on the action $S = S_G + S_F$, where we have used periodic boundary conditions for the gauge fields and periodic (anti-periodic) spatial (temporal) boundary conditions for the fermions. The extent of the lattice in the μ direction will be denoted by L_μ, so that the four-dimensional volume is given by $V = L_1 L_2 L_3 L_4$.

We have performed calculations on 8^4, $8^3 \cdot 16$ and 12^4 lattices at β values ranging between 0.16 and 0.22 and at masses between 0.01 and 0.16. The actual values

can be read off from the forthcoming tables. We have used the hybrid Monte Carlo algorithm [19] for updating the gauge field configurations. Some details of the performance of the algorithm for QED can be found in ref. [1]. On the 12^4 lattices we have accumulated $O(250)$ gauge field configurations, each separated by 5 - 10 trajectories, for each value of β and m. For $m = 0.01$, however, we were only able to accumulate $O(100)$ configurations. On the 8^4 and $8^3 \cdot 16$ lattices our data sample consists of $O(100)$ configurations, each separated by 25 trajectories. The trajectory length τ was chosen to be 0.7 - 1.0, and $\delta\tau$, the molecular dynamics step size, was set so that an acceptance of 70 - 80 % was obtained. On the 12^4 lattices the most time consuming runs were those with $m = 0.01$, when $\delta\tau = 0.007$, $n_s \equiv \tau/\delta\tau = 100$ was chosen. For $m = 0.02$, 0.04 we needed $\delta\tau = 0.0125$, $n_s = 60$ and $\delta\tau = 0.02$, $n_s = 40$, respectively. These are values for $\beta > \beta_c$. For $\beta < \beta_c$, $\delta\tau$ had to be slightly reduced to maintain the acceptance. The stopping criterion for the conjugate gradient inverter was taken as $r^2 < 10^{-10}$.

3 Chiral condensate and phase diagram

The first step in our calculation is the determination of the phase diagram. This includes the determination of the critical coupling and, as far as this is possible, of the critical exponents.

The quantity of main interest here is the chiral condensate $\langle\bar{\chi}\chi\rangle$. To compute $\langle\bar{\chi}\chi\rangle$, we have used a stochastic estimator, as, e.g., employed in ref. [20], which makes use of one inversion of the fermion matrix for a source vector of random numbers of mean zero. The results of the calculation are given in table 1. For completeness we list the average gauge field action per plaquette in table 2.

For $\beta < \beta_c$, where β_c is the critical coupling below which chiral symmetry is spontaneously broken (which will turn out to be $\beta_c = 0.186$), we find that the finite size effects displayed by the data are consistent with the formula

$$\begin{aligned}\langle\bar{\chi}\chi\rangle(m,V) &= \langle\bar{\chi}\chi\rangle(0,\infty)\frac{I_0'(s)}{I_0(s)} \\ &= \langle\bar{\chi}\chi\rangle(0,\infty) - \frac{3}{8mV} + O(V^{-2}),\end{aligned} \tag{3.1}$$

where $s = mV\langle\bar{\chi}\chi\rangle(0,\infty)$ and $I_0(s)$ is the modified Bessel function. This equation was derived by Jolicoeur and Morel [21] in the strong coupling limit, where the symmetry of the action is $U(1) \times U(1)$. In case the chiral $SU(4) \times SU(4)$ symmetry

is restored, the formula of Gasser and Leutwyler [22] applies, which gives a factor of 15/32 instead of 3/8 in eq. (3.1). We conclude from eq. (3.1) and comparison between the 8^4, $8^3 \cdot 16$ and 12^4 lattices that finite size effects are small, and that the extrapolation of $\langle\bar{\chi}\chi\rangle$ to the infinite volume lies within the error bars of the results on the 12^4 lattice. For $\beta > \beta_c$ no such extrapolation formula is known.

In ref. [1] we have given a heuristic derivation of the effective action. The mean field approximation to this (truncated) action gave the equation of state

$$m = 2\kappa\sigma + 4\zeta\sigma^3, \tag{3.2}$$

where $\sigma = \langle\bar{\chi}\chi\rangle$, and κ, ζ are analytic functions of β in the vicinity of the critical point. Recall that in the chiral limit, $m \to 0$, $\sigma = \sqrt{-\kappa/2\zeta}$ if κ is negative and $\sigma = 0$ otherwise. The critical point is the value of β at which κ changes sign. We found that our previous data could well be fitted by eq. (3.2). This we regarded as an indication that the theory is non-interacting in the continuum limit. Closer to the critical point eq. (3.2) can, however, not be expected to hold anymore if our interpretation is correct: it will receive logarithmic corrections, due to renormalization, causing the (renormalized) coupling constant ζ to vanish at the critical point. These corrections can be computed in the $O(n)$-symmetric linear σ model [23] underlying the effective action. As a result, we are led to the following modification of the equation of state (3.2) for small σ:

$$m = \tau\frac{\sigma}{\ln^p|\sigma^{-1}|} + \theta\frac{\sigma^3}{\ln|\sigma^{-1}|}, \tag{3.3}$$

where τ, θ are analytic in β. For $n = 2$, which corresponds to the $U(1) \times U(1)$ symmetry of the original action, one obtains $p = 0.4$. We shall keep p as a free parameter, because we do not know yet what the symmetry is at the critical point, and also for a consistency check of the approach we have taken. Equation (3.3) means that the coupling constant vanishes like $1/\ln|\sigma^{-1}|$.

We have fitted eq. (3.3) to the data on our largest lattices in table 1. The parameters τ, θ have been parametrized as follows:

$$\frac{\tau}{\theta} = \tau_1(1 - \frac{\beta}{\beta_c}), \tag{3.4}$$

$$\frac{1}{\theta} = \theta_0 + \theta_1(1 - \frac{\beta}{\beta_c}). \tag{3.5}$$

The reason for this choice is to guarantee that σ^2 is regular on the axis $m = 0$. The result of the fit is shown in fig. 1. We obtain $\beta_c = 0.186(1)$ and $p = 0.61(1)$.

(For the other parameter values see the caption to fig. 1.) The latter value is roughly what one expects from the renormalization group of the $O(n)$ model, indicating perhaps that the symmetry is higher than $n = 2$. In order to make the critical behavior visible directly, we have shown a slightly modified version of the scaling plot, introduced in ref. [1], in fig. 2. The fact, that the data points fall on a universal curve near the critical point, indicates that eq. (3.3) is a good description of the data. Consequently,

$$\begin{aligned} \sigma \ln^{\frac{\rho-1}{2}}|\sigma^{-1}| &\propto (\beta_c - \beta)^{\frac{1}{2}} \quad \text{for} \quad \beta \leq \beta_c, \\ \sigma &= 0 \quad \text{for} \quad \beta \geq \beta_c \end{aligned} \tag{3.6}$$

on the critical line $m = 0$ and

$$\sigma \ln^{-\frac{1}{3}}|\sigma^{-1}| \propto m^{\frac{1}{3}} \tag{3.7}$$

at $\beta = \beta_c$. We conclude, altogether, that the data are in good agreement with mean field theory plus logarithmic corrections. The significance of logarithmic corrections was also noticed in recent analytic work based on truncated Schwinger-Dyson equations [12].

The shift of β_c relative to our old value [1] is due to the new data points at $m = 0.01$. We have tried to fit our new data by the mean field equation of state (3.2) without logarithmic corrections. This gave a worse fit. However, it should be said that it is possible to fit the data also by an equation of state as given in ref. [24], in which the critical exponents are left as free parameters. Such a fit gave exponents, which differ slightly from the mean field values. That means, it is hard to distinguish between logarithmic and small power corrections. Conclusions drawn from fits to the equation of state alone are thus to be treated with caution. All fits led to compatible values of β_c though. In sect. 10 we shall further discuss the critical exponents.

From the symmetry of the action (2.3) under $m \to -m$ we infer that

$$\lim_{m \searrow 0} \langle \bar{\chi}\chi \rangle = -\lim_{m \nearrow 0} \langle \bar{\chi}\chi \rangle \tag{3.8}$$

for $\beta \leq \beta_c$. Thus, the line $m = 0$, $\beta \leq \beta_c$ is a line of first order phase transitions. In sect. 5 we shall see that the renormalized fermion mass m_R vanishes when $\langle \bar{\chi}\chi \rangle$ vanishes. That is the case on the line $m = 0$, $\beta \geq \beta_c$. As the vanishing mass corresponds to the diverging correlation length $\xi = 1/m_R$, this line is a line of second order phase transitions. Hence, the critical point is a tricritical point separating the first and second order critical lines. The corresponding phase diagram is shown in fig. 3.

The success of the equation of state (3.3) suggests that chiral symmetry breaking is induced by four- and eight-fermion interactions, which are generated dynamically in the strong coupling region. This mechanism of symmetry breaking is similar to that of the Nambu–Jona-Lasinio model [25]. In order that these interactions be relevant in the critical region, the theory must develop large anomalous dimensions.

4 Static potential and phase structure

Before we proceed further, we have to investigate the nature of the different phases. One could think that QED is confining in the chirally broken phase, because the compact $U(1)$ theory is confining at strong coupling. That could question the notion of the renormalized fermion mass as used in ref. [2] and in this work, at least near the first order critical line.

In order to study the different phases, we consider the potential of static test charges. Because of the non-compact nature of the action, we can probe charges of arbitrary (not just integer) strength. The potential derives from the correlation function of Polyakov loops of opposite charges

$$C_q(\vec{x}) = \langle P_q(\vec{x}) P_q^-(\vec{0}) \rangle \tag{4.1}$$

with

$$P_q(\vec{x}) = \exp(iq \sum_{x_4} A_4(x)), \tag{4.2}$$

where q is the external charge (in units of the bare charge e). The Polyakov loop operator (4.2) projects onto states with charge q at position $\vec{x}$. We denote the corresponding eigenvalues of the transfer matrix by $\lambda_q^{(n)}(\vec{x})$. Then we can write

$$C_q(\vec{x}) = Z^{-1} \sum_n (\lambda_q^{(n)}(\vec{x}))^{L_4}, \tag{4.3}$$

$$Z = \sum_n (\lambda_0^{(n)})^{L_4}, \tag{4.4}$$

where the sum may encounter degenerate eigenvalues. The eigenvalues define potentials

$$V_q^{(n)}(\vec{x}) = -\ln(\lambda_q^{(n)}(\vec{x})) + \ln Z. \tag{4.5}$$

We are primarily interested in the ground state potential $V_q^{(0)}(\vec{x})$. Usually, the excited potentials are eliminated by taking L_4 large.[3] Here, however, we can vary q to investigate the influence of excited potentials.

If the potential is dominated by single dressed photon exchange, the ground state potential is expected to be proportional to q^2, i.e.

$$V_q^{(0)}(\vec{x}) = q^2 V(\vec{x}). \tag{4.6}$$

The effective potential can then be written

$$V_q^{eff}(\vec{x}) \equiv -\frac{1}{L_4 q^2}\ln C_q(\vec{x}) = V(\vec{x}) + \frac{1}{L_4 q^2}\ln[1 + \sum_{n>0}(\lambda_q^{(n)}(\vec{x})/\lambda_q^{(0)})^{L_4}]. \tag{4.7}$$

The proportionality (4.6) can be tested, and the contribution of excited potentials be identified and separated, by varying q^2. If the effective potential (4.7) is independent of q^2 in a sufficiently large range of q^2, the contribution of the excited potentials is negligible. In practice the range of q^2 is limited, because the correlation function falls exponentially with q^2 and disappears in the noise for too large values of q^2. A further advantage of variable test charge is that one can tune q^2, such that the statistical errors in $C_q(\vec{x})$ are minimized.

We have investigated the potential on the 8^4 and 12^4 lattices. Here we shall report only on the results obtained on the 12^4 lattices. (The 8^4 lattices gave qualitatively the same results.) The calculation was done for test charges q =0.1, 0.2, 0.3, 0.5 and 1.0 and positions $\vec{x} = (l,0,0)$, $(l,l,0)$, and (l,l,l) with $l = 1, 2, \ldots, 6$. On the 12^4 lattice we did not find any useful signal for $q = 1$.

Let us first look at the q^2 dependence of the effective potential. In fig. 4 we show $V_q^{eff}(\vec{x})$ as a function of q^2 for $\vec{x} = (1,0,0)$, $(1,1,0)$, $(1,1,1)$ and $(6,6,6)$. The bare parameters are $\beta = 0.17$ ($< \beta_c$) and $m = 0.02$, which are close to the first order critical line. We find that $V_q^{eff}(\vec{x})$ is independent of q^2 at all distances. The same was found to be the case for all other values of β and m for $q > 0.2$. On the 8^4 lattices also the $q = 1$ signal is clearly visible at short distances ($\vec{x} = (1,0,0)$, $(1,1,0)$) and consistent with the results at smaller values of q. This indicates that excited potentials are suppressed for our choice of q.

We shall now investigate the potential quantitatively. Since the statistical errors were found to be minimal for $q = 0.3$, we have taken this value in the subsequent analysis. In fig. 5 we show the potential for two sets of bare parameters on either side of the critical point: $\beta = 0.17$, $m = 0.02$ and $\beta = 0.22$ ($> \beta_c$), m = 0.02. We shall try to fit the potential by the lowest order lattice perturbative formula

$$V(\vec{x}) = -\frac{e_{eff}^2}{L_1 L_2 L_3} \sum_{k=(\vec{k},0),\vec{k}\neq\vec{0}} \frac{e^{ikx}}{\hat{k}^2} + E, \tag{4.8}$$

$$E = \frac{e_{eff}^2}{L_1 L_2 L_3} \sum_{k=(\vec{k},0),\vec{k}\neq\vec{0}} \frac{1}{\hat{k}^2} + E_0\,, \tag{4.9}$$

where

$$\hat{k}^2 = \hat{k}_\mu \hat{k}_\mu^*\,,\ \hat{k}_\mu = e^{ik_\mu} - 1. \tag{4.10}$$

The first term on the right-hand side of eq. (4.8) corresponds to the one-photon exchange diagram, whereas E represents the self-energy of the static charges. The effective charge e_{eff}, which we treat as a free parameter, is to be interpreted as the renormalized charge e_R, which we will properly define in sect. 6. The constant E_0 in E accounts for higher order contributions to the self-energy. The fit of eq. (4.8) to the data, with fit parameters e_{eff} and E_0, is shown by the solid symbols in fig. 5. We find that the data are well described by the Coulomb potential (4.8). At short distances the data show some violation of rotational invariance. This effect is also reproduced by the lattice photon propagator. The effective charges obtained from the fit are significantly lower than the bare charges. (See the figure caption for the actual values.) This indicates that the bare charges are screened. The parameter E_0 in the formula for the self-energy contribution, eq. (4.9), turned out to be positive. A positive E_0 means that the potential is steeper than eq. (4.8) at very short distances. This, as well as the systematic deviation from the $|\vec{x}| = 1$ data points, may be interpreted as a first sign of running of the effective coupling constant: the effective charge has to increase at short distances to account for the data. We will present a more accurate determination of the renormalized charge in sect. 6. There we will also show that the potential can be described quantitatively, including the self-energy contribution (i.e. without having to introduce the *ad hoc* constant E_0), by one-loop renormalized perturbation theory.

For integer test charges even a confining potential will flatten off at large distances and eventually look similar to our Coulomb potential in fig. 5, because the external charges can combine with the dynamical charges to form neutral states. In our case of fractional test charges the situation is, however, different. Here, the external charges can only be screened partly, so that in the case of confinement we would still find a rising potential at large distances. This is clearly not what we see. We conclude that non-compact QED does not confine even in the chirally broken phase, contradicting the scenario of ref. [27].

[3] For a discussion of this issue in the context of QCD see, e.g., ref. [26].

5 Fermion propagator and renormalized fermion mass

In this section, we discuss some properties of the fermion propagator and describe our procedure [28] for extracting the renormalized fermion mass m_R.

Since m_R is the mass of a charged particle, its computation is not as straightforward as, e.g., the determination of meson masses in QCD. This is related to the fact that the fermion propagator is not gauge invariant: a bare electron without its Coulomb field (i.e. its surrounding photon cloud) is not a gauge invariant concept. To maintain manifest gauge invariance, one has to study states containing not only the electron but also its Coulomb field.

Thus, we shall calculate the fermion propagator in a fixed gauge, as is done in perturbation theory [29]. The renormalized mass is gauge invariant, as is shown in appendix A. We choose the Landau gauge, defined by the condition

$$\sum_\mu \bar{\Delta}_\mu A_\mu(x) = 0, \tag{5.1}$$

which can be implemented exactly. Here $\bar{\Delta}_\mu$ denotes the backward lattice derivative.

However, the condition (5.1) does not fix all gauge-like degrees of freedom of the action. The action S is also invariant under the transformation

$$\begin{aligned} A_\mu(x) &\rightarrow A_\mu(x) + \Delta_\mu \alpha(x), \\ \chi(x) &\rightarrow e^{-i\alpha(x)}\chi(x), \\ \bar{\chi}(x) &\rightarrow e^{i\alpha(x)}\bar{\chi}(x) \end{aligned} \tag{5.2}$$

with

$$\alpha(x) = \sum_\mu \frac{2\pi}{L_\mu} n_\mu x_\mu, \quad n_\mu \text{ integer}. \tag{5.3}$$

Since $\alpha(x)$ is not a periodic function, this is not a gauge transformation for the A_μ field. It is, however, a gauge transformation for the fermions, because they couple only to the compact link variables: $e^{i\alpha(x)}$ is periodic. Thus, averaging over these transformations would give zero for the fermion propagator.

Obviously, this invariance is not eliminated by the Landau gauge condition. Therefore, we add multiples of $2\pi/L_\mu$ to $A_\mu(x)$, such that the lattice average

$$\bar{A}_\mu = \frac{1}{V}\sum_x A_\mu(x) \tag{5.4}$$

fulfills the condition

$$-\frac{\pi}{L_\mu} < \bar{A}_\mu \leq \frac{\pi}{L_\mu} \tag{5.5}$$

for all μ. After performing this procedure, we calculate the propagator

$$G_\omega(t) = \sum_{\vec{x}} \langle \chi(2x+\omega)\bar{\chi}(0)\rangle. \tag{5.6}$$

Here, x is considered as labeling a hypercube, ω denotes a four-vector with components 0 or 1 and $t = 2x_4 + \omega_4$. That is, we compute the propagator connecting a lattice point, whose coordinates are all even, with all points in the hypercube based at $2x$. The sum over $\vec{x}$ then projects onto zero momentum. In the actual computation we have calculated G_ω for a source distributed over all points with even space coordinates in a given time slice. Subsequently, the average over all times was taken.

The discrete symmetries of staggered fermions restrict $G_\omega(t)$ severely. One finds that $G_\omega(t)$ has to vanish for $\vec{\omega} \neq \vec{0}$, and that $G_{\vec{0}}(t)$ should be real. To see the physical implications of this result, we construct flavored Dirac spinors $\psi_\alpha^{(a)}(2x), \bar{\psi}_\alpha^{(a)}(2x)$ out of the χ and $\bar{\chi}$ fields according to [30]:

$$\psi_\alpha^{(a)}(2x) = \frac{1}{8}\sum_{\omega_\mu=0,1} \chi(2x+\omega)\left(\gamma_1^{\omega_1}\cdots\gamma_4^{\omega_4}\right)_{\alpha a}, \tag{5.7}$$

$$\bar{\psi}_\alpha^{(a)}(2x) = \frac{1}{8}\sum_{\omega_\mu=0,1} \bar{\chi}(2x+\omega)\left(\gamma_1^{\omega_1}\cdots\gamma_4^{\omega_4}\right)^*_{\alpha a}, \tag{5.8}$$

where α is a Dirac index and a is a flavor index. Their propagator (for zero momentum) is then given by

$$\begin{aligned} 16\sum_{\vec{x}}\langle\psi_\alpha^{(a)}(2x)\bar{\psi}_\beta^{(b)}(0)\rangle &= G_{\vec{0}}(2x_4)\delta_{\alpha\beta}\,\delta_{ab} + \tfrac{1}{2}\left(G_{\vec{0}}(2x_4+1) + G_{\vec{0}}(2x_4-1)\right)(\gamma_4)_{\alpha\beta}\,\delta_{ab} \\ &\quad + \tfrac{1}{2}\left(G_{\vec{0}}(2x_4+1) - G_{\vec{0}}(2x_4-1)\right)(\gamma_5)_{\alpha\beta}\,(\gamma_1\gamma_2\gamma_3)_{ab}. \end{aligned} \tag{5.9}$$

The first two terms are proportional to the unit matrix in the space of flavor indices a, b and, hence, are flavor symmetric, whereas the last term breaks flavor symmetry. The existence of flavor breaking contributions on the lattice was, of course, to be expected. However, if the continuum limit of the above propagator exists at all, it will be flavor symmetric, because the non-symmetric term contains the difference of $G_{\vec{0}}(t)$ evaluated at two points separated by two lattice constants without a compensating lattice constant in the denominator, which would lead to a derivative [31].

The numerical data, however, do not exhibit this form of the propagator: we observe non-vanishing values of $G_{\vec{\omega}}(t)$ for $\vec{\omega} = \hat{1}, \hat{2}, \hat{3}$ and an imaginary part in $G_{\vec{0}}(t)$. So, some of the discrete symmetries, which staggered fermions ought to obey, must be violated by our configurations. This turned out to be caused by the fact that $\bar{A}_\mu$ does not average to zero in our ensembles. In fig. 6 we show $\bar{A}_4$ on a 12^4 lattice as a function of computer time for a typical case. Note the jumps of $\bar{A}_4$ due to the constraint (5.5) ($\pi/12 \approx 0.26$). The spatial components of $\bar{A}$ behave in a similar way, in spite of the different fermionic boundary conditions.

So, it is not surprising that the observed propagators do not follow the conclusions drawn from the complete group of discrete symmetries: charge conjugation, lattice rotations and reflections are broken by the non-vanishing background potential $\bar{A}_\mu$. But translational invariance alone suffices to establish flavor symmetry restoration in the continuum limit along the lines indicated above.

The non-vanishing ensemble averages of $\bar{A}_\mu$ could be considered as indicating insufficient statistics. To obtain $\langle \bar{A}_\mu \rangle = 0$, it would, however, probably be necessary to increase the number of configurations at least by a factor of 10 - 100. Since this is far beyond our possibilities, we have to learn to live with $\langle \bar{A}_\mu \rangle \neq 0$. To take the non-vanishing $\langle \bar{A}_\mu \rangle$ into account, we fitted the computed propagators with the propagator in a constant background potential B_μ, restricted to the interval $-\pi/L_\mu < B_\mu \leq \pi/L_\mu$. The only non-zero contributions are

$$
\begin{aligned}
G_{\vec{0}}(2x_4) &= \frac{m_R}{L_4} \sum_{p_4} \mathrm{e}^{2\mathrm{i}p_4 x_4} \left(\sin^2(p_4 + B_4) + \tilde{m}^2 \right)^{-1}, \\
G_{\vec{0}}(2x_4 + 1) &= -\frac{1}{2m_R} \left\{ \mathrm{e}^{\mathrm{i}B_4} G_{\vec{0}}(2x_4 + 2) - \mathrm{e}^{-\mathrm{i}B_4} G_{\vec{0}}(2x_4) \right\}, \qquad (5.10) \\
G_{\vec{j}}(2x_4) &= -\mathrm{i} \frac{\sin B_j}{m_R} G_{\vec{0}}(2x_4), \quad j = 1, 2, 3,
\end{aligned}
$$

where

$$
p_4 = \frac{2\pi}{L_4} n, \; n = \pm\frac{1}{2}, \pm\frac{3}{2}, \ldots, \pm\frac{1}{2}(L_4 - 1), \qquad (5.11)
$$

due to the anti-periodic temporal boundary conditions for the fermions, and

$$
\tilde{m}^2 = m_R^2 + \sum_{j=1}^{3} \sin^2 B_j. \qquad (5.12)
$$

This pattern of non-vanishing contributions is precisely reproduced by the results of the Monte Carlo simulations.

Doing the momentum sum one obtains

$$
\begin{aligned}
G_{\vec{0}}(2x_4) = {} & \frac{2m_R}{\sinh(2\tilde{\mu})} \left[\cosh^2(\tfrac{1}{2}\tilde{\mu}L_4) - \sin^2(\tfrac{1}{2}B_4 L_4) \right]^{-1} \\
& \times \Big\{ \Big[\cos(\tfrac{1}{2}B_4 L_4) \cosh(\tfrac{1}{2}\tilde{\mu}L_4) \cos(B_4(\tfrac{1}{2}L_4 - 2x_4)) \sinh(\tilde{\mu}(\tfrac{1}{2}L_4 - 2x_4)) \\
& + \sin(\tfrac{1}{2}B_4 L_4) \sinh(\tfrac{1}{2}\tilde{\mu}L_4) \sin(B_4(\tfrac{1}{2}L_4 - 2x_4)) \cosh(\tilde{\mu}(\tfrac{1}{2}L_4 - 2x_4)) \Big] \qquad (5.13) \\
& + \mathrm{i} \Big[\cos(\tfrac{1}{2}B_4 L_4) \cosh(\tfrac{1}{2}\tilde{\mu}L_4) \sin(B_4(\tfrac{1}{2}L_4 - 2x_4)) \sinh(\tilde{\mu}(\tfrac{1}{2}L_4 - 2x_4)) \\
& - \sin(\tfrac{1}{2}B_4 L_4) \sinh(\tfrac{1}{2}\tilde{\mu}L_4) \cos(B_4(\tfrac{1}{2}L_4 - 2x_4)) \cosh(\tilde{\mu}(\tfrac{1}{2}L_4 - 2x_4)) \Big] \Big\},
\end{aligned}
$$

where $\sinh\tilde{\mu} = \tilde{m}$ and $0 \leq 2x_4 < L_4$. Note that $\mathrm{Im}\, G_{\vec{0}}(t)$ changes sign if B_4 jumps from $-\pi/L_4$ to $+\pi/L_4$.

Fitting the computed values of $G_{\vec{0}}(t)$ with the above expression, we have four free parameters: $\sum_{j=1}^{3} \sin^2 B_j$, B_4, m_R and an overall amplitude. We did not attempt to fit also $G_{\vec{j}}$ ($j = 1, 2, 3$), although the numerical results appear to be consistent with the relation (5.10). Note that m_R is given by the ratio of even to odd time propagators.

Since the lattice average $\bar{A}_\mu$ does vary (though slowly) from configuration to configuration, we divided our ensembles into sets of 10 - 20 consecutive configurations. Sets which included jumps of $\bar{A}_4$ by $2\pi/L_4$ did not, in general, allow for stable fits and so have been discarded. The masses are obtained by averaging the masses found from each set. Fits to $G_{\vec{0}}(t)$ starting from the initial points $t_0 = 1, 2, 3$ gave consistent results, and for our final estimates, which are given in table 3, we took the results obtained using $t_0 = 1$. Moreover, the fitted values of B_4 and of $\sum_{j=1}^{3} \sin^2 B_j$ are found to agree very well with the (directly) computed values of $\bar{A}_\mu$. The overall amplitude turned out to be about one, which indicates that the fermion wave function renormalization constant is $Z_2 \approx 1$. Note that in Landau gauge $Z_2 = 1 + O(e_R^4)$. If the theory were confining for $\beta < \beta_c$, we would expect $Z_2 = 0$ in this region. Typical fits of Re $G_{\vec{0}}(t)$ and of Im $G_{\vec{0}}(t)$ on the 12^4 lattice for $\beta = 0.17$, $m = 0.02$ and $\beta = 0.22$, $m = 0.02$ are shown in figs. 7 and 8, respectively. The solid lines belong to even t, whereas the dashed lines are the fit for odd values of t.

For an alternative calculation of the fermion mass see appendix B. No significant differences were found.

Having found the renormalized mass, we may now confront it with the chiral condensate. In fig. 9 we have plotted $\langle\bar{\chi}\chi\rangle$ as a function of m_R. We make the observation that the data lie on a universal curve. This indicates that $\langle\bar{\chi}\chi\rangle$, although being an unrenormalized quantity, is a function of m_R alone. The dashed curve in fig. 9 shows the contribution of a free fermion of mass m_R on an infinite lattice, i.e.

$$\langle\bar{\chi}\chi\rangle = \int_{-\pi}^{+\pi} \frac{d^4p}{(2\pi)^4} \frac{m_R}{\sum_\mu \sin^2 p_\mu + m_R^2}. \tag{5.14}$$

It is legitimate to compare the data with this formula, because the data are practically indistinguishable from the infinite volume extrapolation, as we noted earlier on. Since in this limit the background fields disappear, we can ignore them here. For a more detailed discussion see appendix C. For small m_R eq. (5.14) gives

$$\langle\bar{\chi}\chi\rangle = 0.6197\, m_R + O(m_R^3 \ln m_R^2). \tag{5.15}$$

We find good agreement between the data and this curve for $m_R \lesssim 0.5$. Including a fermion wave function renormalization constant in eq. (5.14) would rescale this ratio of proportionality by a factor of Z_2. The success of (5.15) tells us that $Z_2 \approx 1$ for small m_R, as we also found in our fit to the fermion propagator.

The fact, that $\langle\bar{\chi}\chi\rangle$ and m_R are related in the same way on both sides of β_c, suggests that the main effect of the chiral transition is simply to give the fermion a mass, which acts in the same way as the mass introduced by m in the symmetric phase. The Miransky model [7] predicts $\langle\bar{\chi}\chi\rangle \propto m_R^2$ near the phase transition. We see no sign of such behavior but find $\langle\bar{\chi}\chi\rangle \propto m_R$ at all values of β. Naively, i.e. assuming for the moment that $\bar{\chi}\chi$ does not mix under renormalization, we would conclude from this that $\bar{\chi}\chi$ has dimension one, as is also suggested by the mean field equation of state (3.3). We shall return to this question in sect. 10.

The proportionality of $\langle\bar{\chi}\chi\rangle$ and m_R for sufficiently small values of m_R leads, through eq. (3.3), to the scaling laws

$$\begin{aligned} m_R &\propto (\beta_c - \beta)^{\frac{1}{2}} \quad \text{for} \quad \beta \le \beta_c, \\ m_R &= 0 \qquad\quad \text{for} \quad \beta \ge \beta_c \end{aligned} \tag{5.16}$$

on the critical line $m = 0$ and

$$m_R \propto m^{\frac{1}{4}} \tag{5.17}$$

at $\beta = \beta_c$, up to logarithmic corrections.

We shall now discuss the nature of chiral symmetry breaking in QED, which, as we shall see, is quite different from QCD. When chiral symmetry breaks in

QCD, the fermion self-energy $\Sigma(p)$ at low momenta acquires a large value, but at momenta large compared with Λ_{QCD} the part of $\Sigma(p)$ due to chiral symmetry breaking drops off like $1/p^2$; see fig. 10. If the scalar part of the fermion propagator does behave this way, the integral for the bare chiral condensate (in continuum notation for N_f flavors and momentum cut-off Λ)

$$\langle\bar{\psi}\psi\rangle = \int_0^\Lambda \frac{d^4p}{(2\pi)^4} \frac{4N_f\Sigma(p)}{C(p)(p^2+\Sigma(p)^2)} \tag{5.18}$$

will be only logarithmically divergent (because the integrand goes as $1/p^4$). This sort of chiral symmetry breaking is known as soft breaking of chiral symmetry [32]. For small masses m we would find that the chiral condensate was proportional to Λ_{QCD}^3. Hard breaking of chiral symmetry, as seen for example in the bubble aproximation to the Nambu–Jona-Lasinio model [25], leads to a $\Sigma(p)$ with less momentum dependence (perhaps logarithmic). The above integral (5.18) for the chiral condensate looks much more like the free fermion integral (5.14). Hard breaking of chiral symmetry leads to a chiral condensate proportional to m_R (up to logarithmic corrections). This is what we see in fig. 9. We conclude that chiral symmetry breaking in QED is hard.

An intermediate case is provided by the critical behaviour predicted by Miransky [7]. In the Miransky solution $\Sigma(p)$ drops off like $1/p$ at large momenta, and $\langle\bar{\psi}\psi\rangle$ is proportional to m_R^2.

6 Renormalized charge

We now come to the problem of computing the renormalized charge. In ref. [2] we did not give any details or tables of the results, while in ref. [33] the method was only sketched. In this section we shall describe in some detail our approach to this problem. We have used two different methods. One proceeds via the photon propagator, and the other via the potential.

Photon propagator

Whether we have a lattice or gauge invariant continuum regularization, the Ward identities are preserved. This means that the fermion wave function renormalization constant Z_2 is equal to Z_1, the vertex renormalization constant, and so the

charge renormalization is given only by the photon wave function renormalization constant Z_3. Thus we have

$$e_R^2 = Z_3 e^2, \tag{6.1}$$

where e_R is the renormalized charge. So, we can write, after fixing the gauge,

$$\frac{\beta}{V}\langle \tilde{A}_\mu(k)\tilde{A}_\nu^*(k)\rangle = \frac{Z_3}{\hat{k}^2}\left[\delta_{\mu\nu} - (1-\lambda_R)\frac{\hat{k}_\mu \hat{k}_\nu^*}{\hat{k}^2}\right] + \dots , \tag{6.2}$$

where $\tilde{A}_\mu(k)$ is the Fourier transform of $A_\mu(x)$, λ_R is the renormalized gauge fixing parameter and the dots in eq. (6.2) represent terms that are not singular as $k \to 0$. The β factor is due to the lattice definition of the action (2.1). Equation (6.2) is equivalent to

$$Z_3 = \lim_{k\to 0} D(k), \tag{6.3}$$

where

$$D(k) = \beta \frac{1}{N_k V}\sum \hat{k}^2 \langle \tilde{A}_\mu(k)\tilde{A}_\mu^*(k)\rangle|_{k_\mu = 0}. \tag{6.4}$$

The right-hand side of eq. (6.4) is simply the gauge invariant piece of the photon propagator, as we choose the direction μ with $k_\mu = 0$. $D(k)$ is taken as a function of $k^2 = k_\mu k_\mu$ with $k_\mu = 2\pi n_\mu / L_\mu$, $n_\mu = 0, \dots, L_\mu - 1$. The sum extends over all directions μ and for each μ over all momenta k, such that $k_\mu = 0$ and k^2 is fixed, giving N_k possibilities. (Thus, for example for $n^2 = 1, 2, 3, 4, 5, 6, 7, 8$ we have $N_k = 4, 6, 4, 4, 12, 12, 0, 6$ respectively.) We use a lattice propagator in our definition of Z_3, because we shall later find that a comparison with the numerical results leads to a far greater k region of applicability.

Let us now consider a plot for $D(k)$. In fig. 11 we show $1 - D(k)$ against k^2 for $\beta = 0.17$, $m = 0.02$. We see that there is considerable fluctuation of the data, especially for small k^2. It is clearly very difficult, if not impossible, to try to extrapolate to $k = 0$. The fluctuations are an inherent difficulty in computing the A_μ fields directly.

Thus, we have abandoned computing Z_3 via the photon-photon correlation function. Following ref. [34] and exploiting the fact that the integral of a derivative vanishes, we find for an arbitrary operator Ω

$$-\beta\langle \bar{\Delta}_\rho F_{\mu\rho}(x)\Omega\rangle + \frac{\beta}{\lambda}\Delta_\mu\langle \bar{\Delta}_\nu A_\nu(x)\Omega\rangle = \langle j_\mu(x)\Omega\rangle - \langle \frac{\partial \Omega}{\partial A_\mu(x)}\rangle, \tag{6.5}$$

where the lattice current $j_\mu(x)$ is defined by

$$j_\mu(x) = \frac{\partial}{\partial A_\mu(x)}\sum_{y,z}\bar{\chi}(y)M_{yz}\chi(z). \tag{6.6}$$

(From the Ward identity, i.e. invariance of the action under gauge transformations, ref. [34], we have $\lambda_R = \lambda/Z_3$). We now evaluate eq. (6.5) for $\Omega = A_\mu(0)$. Taking the Fourier transform and summing appropriately, we can relate the left hand side of eq. (6.5) with eq. (6.2) or (6.4) to give

$$D(k) = 1 - \frac{1}{N_k V}\sum \langle \tilde{j}_\mu(k)\tilde{A}_\mu^*(k)\rangle|_{k_\mu = 0}. \tag{6.7}$$

The fluctuations of the current will turn out to be smaller than those of the photon field.

However, we have the technical problem of numerically evaluating eq. (6.7), as this involves a fermion correlation function. The current $j_\mu(x)$ in eq. (6.6) is equivalent to

$$j_\mu(x) = -\frac{\partial}{\partial A_\mu(x)}\widetilde{\mathrm{Tr}}\ln Q = -\widetilde{\mathrm{Tr}}\left(Q^{-1}\frac{\partial Q}{\partial A_\mu(x)}\right), \tag{6.8}$$

where $Q = M^\dagger M$, and $\widetilde{\mathrm{Tr}}$ is the trace over the even lattice sites (e) only. This current can be (economically) computed by use of a stochastic estimator (see, e.g., ref. [20]). Thus, if we take ξ as complex Gaussian distributed random numbers with $\langle \xi_x\rangle_\xi = 0$ and $\langle \xi_x \xi_y^\dagger\rangle_\xi = \delta_{xy}$, then

$$j_\mu(x) = -\frac{1}{R}\sum_{r=1}^{R}\widetilde{\mathrm{Tr}}\left(\eta^{(r)\dagger}\frac{\partial Q}{\partial A_\mu(x)}\eta^{(r)}\right), \tag{6.9}$$

where $\eta_e^{(r)} = \sum_{e'} Q_{ee'}^{-1}(M^\dagger \xi^{(r)})_{e'}$. (It can be easily seen that $\langle j_\mu(x)\rangle_\xi = j_\mu(x)$.) Thus, we take R sets of random numbers and evaluate each $\eta_e^{(r)}$ using the conjugate gradient inverter. Although the current is not quite as well localized as the chiral condensate, we would still expect that the averaging produces an acceptable estimator for $j_\mu(x)$. We have checked this point by evaluating $1 - D(k)$ at the smallest value of k^2 as a function of R. A typical result is shown in fig. 12. (See also ref. [33].) We have usually taken $R = 50$ - 100, which proved satisfactory. The slow oscillations of the average can only be suppressed for ridiculously large values of R. However, this is not critical because they always lie within the error bars. In fig. 13 we plot $1 - D(k)$ against k^2 for $\beta = 0.17$, $m = 0.02$ and $\beta = 0.22$, $m = 0.02$. The new correlators fluctuate much less than the old ones, and hence offer a better prospect of finding Z_3.

It is apparent that no matter how we find $D(k)$, we still have the problem of the extrapolation $k \to 0$. We have considered two methods, an extrapolation motivated by renormalized perturbation theory and a simple polynomial fit. The use of renormalized perturbation theory will be justified later.

For the first method we need the polarization tensor $\Pi_{\mu\nu}(k, m_R, V)$. In one-loop order this is given by [4]

$$\Pi_{\mu\nu}(k, m_R, V) = \frac{1}{V}\sum_p \Big\{ -\delta_{\mu\nu}\frac{s_\mu^2(p)}{K(p)} + \frac{c_\mu(p+k/2)c_\nu(p+k/2)}{K(p+k)K(p)} \times \Big[\delta_{\mu\nu}\Big(\sum_\rho s_\rho(p+k)s_\rho(p) + m_R^2\Big) - 2s_\mu(p+k)s_\nu(p)\Big]\Big\}, \tag{6.10}$$

where

$$s_\mu(p) = \sin p_\mu,\ c_\mu(p) = \cos p_\mu,$$
$$K(p) = \sum_\mu s_\mu^2(p) + m_R^2. \tag{6.11}$$

We find this formula better than the corresponding continuum formula, because it includes certain lattice effects, such as the dependence of $\Pi_{\mu\nu}$ on the direction (and not only on the magnitude) of k. Furthermore, it can represent the data when $k \approx \pi$ (the cut-off). We first see that $\Pi_{\mu\nu}(0, m_R, V) \neq 0$ on a finite lattice, which appears to give the photon a mass. This, like all finite size effects, is small on our lattices ($\propto \exp(-m_R L_\mu)$). To avoid this problem, we shall in future make the replacement $\Pi_{\mu\nu}(k, m_R, V) \to \Pi_{\mu\nu}(k, m_R, V) - \Pi_{\mu\nu}(0, m_R, V)$. (See also ref. [36,37]). Performing one-loop perturbation theory for the photon propagator and then projecting out the appropriate component gives

$$\frac{1}{e^2 D(k)} = \frac{1}{e^2} - \Pi(k, m_R, V), \tag{6.12}$$

where

$$\Pi(k, m_R, V) = \frac{1}{N_k}\sum \frac{1}{\hat{k}^2}\left[\Pi_{\mu\mu}(k, m_R, V) - \Pi_{\mu\mu}(0, m_R, V)\right]|_{k_\mu = 0}. \tag{6.13}$$

Now, from the definition of e_R^2 (in eqs. (6.1), (6.3)) we have

$$\frac{1}{e_R^2} = \frac{1}{e^2} - \Pi(0, m_R, \infty), \tag{6.14}$$

and hence

$$\frac{1}{e^2 D(k)} = \frac{1}{e_R^2} + \Pi(0, m_R, \infty) - \Pi(k, m_R, V). \tag{6.15}$$

Equation (6.15) is the formula that we shall fit to the numerical results, because we expect this to keep the higher order terms as small as possible. In this form we have one unknown parameter, namely $1/e_R^2$. Indeed, the formula provides a stringent test, as for each individual k we could make the fit. However, we shall attempt to fit for all k paying special attention to the low momentum modes.

[4] For QCD this was given in ref. [35].

In fig. 13 we show fits of $1 - D(k)$ for $\beta = 0.17$, $m = 0.02$ and $\beta = 0.22$, $m = 0.02$. In general the fit is quite good. As noted above, the fit is for all values of k, which is a hint that one loop renormalized perturbation theory is valid over a large range of distances. The result is not too sensitive to the large momenta, as fitting for half the modes or less does not change appreciably the value of e_R^2. The resulting values of e_R^2 are given in table 4. The agreement between the results on the 8^4 and 12^4 lattices indicates that eq. (6.15) is a good extrapolation formula.

We have also compared our data with Π including background fields. See appendix C. The change in e_R^2 was insignificant.

To check the quality of our results, we have made a polynomial fit (in k^2) to the data. This is done by including higher and higher terms in the polynomial until a plateau is reached, where adding a new term does not bring a significant improvement in the χ^2 per degree of freedom. Usually, three to five terms are needed. A typical graph is shown in fig. 14. This gives results in agreement with use of the fit formula (6.15). However, the errors are in general larger.

Potential

In sect. 4 we have determined the potential and the effective coupling constant at the tree level. The values obtained are consistent with the results in table 4, however, with greater fluctuations. For example, the values obtained from fig. 5 compare favorably with the appropriate results given in the table.

We can now include one-loop corrections. This is done by making the replacement

$$\frac{1}{\hat{k}^2} \to \frac{1}{\hat{k}^2}\frac{1}{1 + e_R^2[\Pi(0, m_R, \infty) - \Pi(k, m_R, V)]}, \tag{6.16}$$

in eqs. (4.8), (4.9) and dropping the constant E_0. It gives the potential

$$V(\vec{x}) = -\frac{e_R^2}{L_1 L_2 L_3}\sum_{k=(\vec{k},0),\vec{k}\neq\vec{0}} \frac{e^{ikx}}{\hat{k}^2}\frac{1}{1 + e_R^2[\Pi(0, m_R, \infty) - \Pi(k, m_R, V)]} + E, \tag{6.17}$$

$$E = \frac{e_R^2}{L_1 L_2 L_3}\sum_{k=(\vec{k},0),\vec{k}\neq\vec{0}} \frac{1}{\hat{k}^2}\frac{1}{1 + e_R^2[\Pi(0, m_R, \infty) - \Pi(k, m_R, V)]}. \tag{6.18}$$

The main effect of this substitution will be to give a better description of the $|\vec{x}| = 1$ data points and the self-energy contribution. In fig. 15 we show the potential together with the prediction of eqs. (6.17), (6.18). The value of e_R^2 is taken from table 4. We find that the potential is well described by one-loop renormalized perturbation theory. At very small m_R we observe some small deviations from one-loop renormalized perturbation theory though. They manifest themselves mainly in a displacement of the point $|\vec{x}| = 1$ and a small shift in E. The shift is an order of magnitude smaller than E_0, the shift needed for the tree-level potential (4.8), (4.9). This shift may signal a two-loop contribution.

We conclude that, within errors, we have agreement between the two methods of determining the renormalized charge.

7 Renormalization group flow and β function

We are interested now in the renormalized charge at the critical point. The cut-off dependence of e_R is described by the Callan-Symanzik β function

$$m_R \frac{\partial e_R^2}{\partial m_R}\bigg|_{e \text{ fixed}} = \beta(e_R^2, m_R), \tag{7.1}$$

where $1/m_R$ acts as the cut-off. (Recall that m_R is given in units of the inverse lattice spacing.) The bare β function $\beta_0(e^2, m_R)$ is defined by

$$-\, m_R \frac{\partial e^2}{\partial m_R}\bigg|_{e_R \text{ fixed}} = \beta_0(e^2, m_R). \tag{7.2}$$

It describes how the bare charge must run in order to keep the renormalized charge constant.

If the critical point is a non-trivial fixed point, the Callan-Symanzik β function must have a second (ultraviolet stable) zero at $e_R^2 = e_R^{*2}$, $m_R = 0$ for $e_R^* \leq e_c$, where $e_c = 1/\sqrt{\beta_c}$. The bound on e_R^* follows from the fact that [38,34] $Z_1 \leq 1$. The bare β function must have a second zero at $e^2 = e_c^2$, $m_R = 0$ in this case. If, on the other hand, QED is trivial, we expect the Callan-Symanzik β function to be given by renormalized perturbation theory near the critical point. For staggered fermions ($N_f = 4$) we obtain on an infinite lattice to one-loop order, combining eq. (7.1) with eq. (6.10),

$$\beta(e_R^2, m_R) = \frac{2}{3} e_R^4 m_R^2 \int_{-\pi}^{\pi} \frac{\mathrm{d}^4 p}{(2\pi)^4} \left[\frac{4c_1^2(p) - c_1^2(p)c_4^2(p) - 1}{K^3(p)} \right]. \tag{7.3}$$

It is easy to check that eq. (7.3) gives

$$\beta(e_R^2, 0) = \frac{2e_R^4}{3\pi^2}, \tag{7.4}$$

i.e. the continuum β function for four flavors. Up to two loops $\beta_0(e^2, m_R) = \beta(e^2, m_R)$, because the first two terms in the expansion of the β function are universal.

The data in tables 3, 4 are plotted in figs. 16 - 18. In fig. 16 we show, motivated by the success of perturbation theory, $1/e_R^2 - 1/e^2$ as a function of m_R. The data points fall, within a few per cent, on a universal curve. Note in particular that the data show the same behavior for $\beta > \beta_c$ (open symbols) and $\beta < \beta_c$ (solid symbols). Exact universality would mean a relationship between e_R and e as given by perturbation theory to one-loop order. The Callan-Symanzik β function is found by differentiating the data. The result is shown in fig. 17 together with the one-loop lattice formula (7.3). At smaller values of m_R (i.e. larger cut-offs and smaller e_R) the observed β function is the same as the one-loop β function, whereas at larger values of m_R there is room for $\lesssim 10$ % contributions from higher orders. The corresponding graph for the normalized bare β function looks almost identical to fig. 17. The dashed curve in fig. 16 is obtained by integrating the renormalization group equations (7.1), (7.2), using the one-loop β functions as input. This gives

$$\frac{1}{e_R^2} - \frac{1}{e^2} = -\Pi(0, m_R, \infty) \tag{7.5}$$

$$= -\int^{\ln m_R} d\ln \bar{m}_R \, \beta(e_R^2, \bar{m}_R)/e_R^4. \tag{7.6}$$

As we saw in fig. 17, the β function at large m_R is not exactly given by the one-loop formula. As we are interested in extrapolating our data to lower values of m_R, we have fixed the implicit integration constant in eq. (7.6), such that the curve fits the data point at the lowest value of m_R. (The shift this amounts to in eq. (7.5) is, however, very small: 0.0017 at $m_R = 0.145$, which is of about the size of the symbols in fig. 16.) There is good agreement between the data and the one-loop result for $m_R \lesssim 0.7$. In fig. 18 we show the lines of constant renormalized charge in the plane of bare parameters β, m. As we know e_R only on a grid of points, we had to interpolate between them. For the interpolation in β and m we have used the formulae $1/e_R^2 = a + b\beta$ and $1/e_R^2 = c + d \ln m$, respectively. (The latter formula is suggested by fig. 16, given the relationship (5.17) near the critical point.) The uncertainty is about 5 % of the spacing between the trajectories. When m, and so m_R, is decreased, β must always be decreased to keep e_R constant, as a result of

the fact that the β function is positive over the entire parameter range. We may use eq. (7.6) to extrapolate the data down to $m = 0$. For $\beta \geq \beta_c$, m_R vanishes as $m \to 0$, and so we obtain that $e_R = 0$ in this limit. (See fig. 16.) In particular, $e_R = 0$ at the critical point. For $\beta < \beta_c$, m_R stays finite as $m \to 0$, and so we obtain a finite charge renormalization. Therefore, all trajectories with finite e_R must end at $m = 0$ on the first order critical line, while $e_R = 0$ on the second order critical line.

This implies that for any finite e_R there is a limit on the cut-off. From eq. (7.6) we obtain, for small m_R,

$$m_R \approx 1.37 \exp\Big(-\frac{3\pi^2}{2}\Big[\frac{1}{e_R^2} - \frac{1}{e^2}\Big]\Big), \tag{7.7}$$

where the factor in front of the exponential can be read off from tables 3, 4 or fig. 16. According to the small m_R expansion of eq. (7.5), we would find the pre-exponential factor in eq. (7.7) to be 1.3646. To find the bound for small e_R, one substitutes e^2 by e_c^2 in eq. (7.7), because the small e_R trajectories end near the critical point. This gives

$$m_R \gtrsim 21.54 \exp\Big(-\frac{3\pi^2}{2e_R^2}\Big). \tag{7.8}$$

Equation (7.8) implies a cut-off, which is an order of magnitude smaller than that implied by the Landau pole.

Taking the lattice spacing to be π over the Planck mass, the bound (7.8) is not nearly saturated in nature, even if one considers all known elementary charged particles. It tells us though that the fine structure constant $\alpha_R = e_R^2/4\pi$ cannot be larger than $\approx 1/50$, because a larger α_R would not allow charged fermions as light as those we see. This assumes that the integration constant does not change drastically when going from four to eight flavors (eight is the sum of the charges squared in the standard model with three generations), and that the cut-off can be pushed to the Planck scale without hitting new physics.

In fig. 18 we have also shown the line $\pi/m_R = 5$, which corresponds to a momentum cut-off of five times the fermion mass. It gives an idea of how close we are to the continuum limit. The largest cut-off we have reached is $\pi/m_R \approx 22$.

Compared with lattice QCD standards, this is a large cut-off, while it remains rather modest in physical terms. Nevertheless, because we have entered the domain of renormalized perturbation theory, we could make statements about the behavior of the theory at the critical point.

8 Fermion-antifermion composite states

In order to study fermion-antifermion composite states, we have calculated (the connected part of) correlation functions of the local operators, which are well known from the computation of meson masses in QCD. These correlation functions have been parametrized in the following way:

$$\begin{aligned} C(t) &= \langle \bar{\chi}(0)\chi(0) \sum_{\vec{x}} s(\vec{x},t)\bar{\chi}(\vec{x},t)\chi(\vec{x},t)\rangle \\ &= A_1\left(\mathrm{e}^{-m_1 t} + \mathrm{e}^{-m_1(L_t-t)}\right) + (-1)^t A_2\left(\mathrm{e}^{-m_2 t} + \mathrm{e}^{-m_2(L_t-t)}\right). \end{aligned} \tag{8.1}$$

The factors $s(\vec{x},t)$, corresponding to different irreducible representations of the lattice symmetry group, together with the standard (continuum) quantum number assignments, are given below:

$s(\vec{x},t)$	particle 1	particle 2
$(-1)^{x_1+x_2+x_3+t}$	$0_{\mathbf{a}}^{-+}(PS)$	$0_{\mathbf{a}}^{+-}(\bar{S})$
$(-1)^t$	$0_{\mathbf{a}}^{-+}(\widetilde{PS})$	$0_{\mathbf{t}}^{++}(S)$
$\frac{1}{3}((-1)^{x_1+x_2}+(-1)^{x_1+x_3}+(-1)^{x_2+x_3})(-1)^t$	$1_{\mathbf{a}}^{--}(V)$	$1_{\mathbf{a}}^{+-}(T)$
$\frac{1}{3}((-1)^{x_1}+(-1)^{x_2}+(-1)^{x_3})(-1)^t$	$1_{\mathbf{a}}^{--}(\tilde{V})$	$1_{\mathbf{a}}^{++}(A)$

(8.2)

The index a (t) refers to the adjoint (trivial) representation of the flavor symmetry group SU(4), and PS, S, V, A and T refer to pseudoscalar, scalar, vector, axial vector and axial vector (with opposite charge conjugation) particles. If flavor symmetry is restored, the states with the same continuum quantum number assignments should have the same mass.

The PS-$\bar{S}$ correlation function is shown in fig. 19. We find that it is dominated by the pseudoscalar state, which is the Goldstone boson associated with the spontaneous breakdown of the axial U(1) symmetry. No contribution of $\bar{S}$ is observed. So, we performed in this case only a two-parameter fit. The results from fits starting at $t_0 = 1$ are shown in table 5. The mass m_{PS} becomes small approaching the first order critical line, as one expects for the mass of a Goldstone boson. Fits starting from $t_0 = 3$ lead to slightly lower masses (different by less than 5 %) in the region of small m and large β ($> \beta_c$), indicating that the overlap of the local operator with the wave function of the Goldstone boson is not as high as it seems to be in the rest of the parameter space explored. Notice also that

m_{PS} exceeds $2m_R$ at $m = 0.01$, $\beta = 0.21$ and at $m = 0.02$, $\beta = 0.22$. Presumably, in this region we are dealing with an unstable particle.

The $\widetilde{PS}-S$ correlation function is shown in fig. 20. The $\widetilde{PS}$ state has the same quantum numbers as the Goldstone boson (PS). So, flavor symmetry restoration would imply $m_{\widetilde{PS}} = m_{PS}$. We were not able to check this relation on our configurations, because the amplitude of $\widetilde{PS}$ becomes very much smaller than the amplitude of S as m gets smaller. So, a reliable $\widetilde{PS}$ mass cannot be extracted. On the other hand, the S signal is surprisingly clean. The results for m_S are given in table 5. However, since S has the quantum numbers of the vacuum, the disconnected part of the correlation function should also be taken into account. Thus, the above results could be modified by annihilation contributions. Note that such contributions could also appear in the other channels. It is generally assumed that they are small in the adjoint channels.

We have made preliminary estimates of the masses corresponding to the remaining correlation functions. The T and A masses are rather large. The V and $\widetilde{V}$ masses are found of order one, decreasing as one approaches the second order critical line (including the critical point), but not as rapidly as m_R. Flavor symmetry restoration need not be good for masses comparable with the cut-off. We find in most cases that $m_{\widetilde{V}}$ exceeds m_V by about 15 %. We plan to return to this point in the future.

The high masses indicate that the fermion-antifermion composite states are not related to positronium-like bound states of the various fermion flavors. Indeed, calculating the Bohr radius, $r_B = 8\pi/(e_R^2 m_R)$, for two particles of mass m_R and charge e_R, one finds values ranging from ≈ 4 at $\beta = 0.16$, $m = 0.16$ to ≈ 45 at $\beta = 0.22$, $m = 0.02$. So, it seems very improbable that the signals observed in the local correlation functions have anything to do with 'positronium'. This is particularly true in that part of the phase diagram explored so far, where we expect to be closest to an approximate scaling region, i.e. for larger values of β and smaller values of m.

We would now like to understand the data. In sect. 3 we have found that an equation of state motivated by the $O(n)$-symmetric linear σ model could describe the behavior of the chiral condensate. In ref. [1] we also analyzed the Goldstone boson in this context. We now are going to extend this to include logarithmic corrections and confront this with our new data, now also including the scalar particle.

The effective action was taken to be

$$S_{eff} = \sum_x \Big\{ \eta \Big[(\Delta_\mu \sigma_x)^2 + (\Delta_\mu \pi_x)^2 \Big] - m\sigma_x + V_{eff}(\sigma_x^2 + \pi_x^2) \Big\}, \tag{8.3}$$

where V_{eff} is the effective potential. From this we derive the equation of state

$$m = 2\sigma V'_{eff}(\sigma^2) = \tau \frac{\sigma}{\ln^p|\sigma^{-1}|} + \theta \frac{\sigma^3}{\ln|\sigma^{-1}|}, \tag{8.4}$$

which we have identified with eq. (3.3). The coefficients of the quadratic terms in the expansion of V_{eff} about the minimum of the effective action give the masses as

$$m_{PS}^2 = \frac{V'_{eff}(\sigma^2)}{\eta}, \tag{8.5}$$

$$m_S^2 = \frac{1}{\eta} \Big\{ V'_{eff}(\sigma^2) + 2\sigma^2 V''_{eff}(\sigma^2) \Big\}. \tag{8.6}$$

Note that a free propagator would lead to an exponential fall-off of the form $\exp(-\sqrt{2(\cosh m_{PS,S} - 1)}\, t)$, rather than $\exp(-m_{PS,S}\, t)$ as used in eq. (8.1). However, the corresponding changes in the plots are not significant.

We allow the wave function renormalization constant η to diverge asymptotically like a power of $\ln\sigma$. Thus, we have for the pseudoscalar mass, writing $\eta = \omega \ln^q|\sigma^{-1}|$,

$$m_{PS}^2 = \frac{m}{2\omega\sigma \ln^q|\sigma^{-1}|}. \tag{8.7}$$

We have fitted eq. (8.7) to our data and found $q = 0.50(5)$, $\omega = 0.15(2)$. In fig. 21 we plot m_{PS}^2 against $m/\sigma\ln^{0.5}|\sigma^{-1}|$. The data points lie on a line in agreement with the effective action and the behavior one expects from Goldstone's theorem.

Let us turn now to the scalar particle and consider

$$\begin{aligned} m_S^2 - m_{PS}^2 &= \frac{2}{\eta}\sigma^2 V''_{eff}(\sigma^2) \\ &= \frac{2\sigma^2}{\eta} \Big\{ \frac{p\tau}{4\sigma^2 \ln^{p+1}|\sigma^{-1}|} + \frac{\theta}{2\ln|\sigma^{-1}|} + \frac{\theta}{4\ln^2|\sigma^{-1}|} \Big\}. \end{aligned} \tag{8.8}$$

There are no undetermined parameters remaining. In fig. 22 we have plotted $m_S^2 - m_{PS}^2$ against the right-hand side of eq. (8.8). For the smaller masses the agreement between our data and the prediction of the effective action is reasonably

good. We find that $m_S^2 - m_{PS}^2$ goes to zero in the chiral limit, as required by chiral symmetry.

Summarizing, we may say that the pseudoscalar and scalar masses together with the chiral condensate are quite well described by the effective action (8.3), which treats σ_x and π_x as elementary fields.

An obvious extension of this model is to couple the fermion in with a chirally invariant Yukawa coupling, just as in the original σ model of Gell-Mann and Levy [39].

9 To what extent is QED renormalizable?

Before we discuss our results, we shall introduce some notions. A theory is renormalizable, if, when the cut-off is varied, the physics can be kept constant by making appropriate changes in the bare parameters. We call a theory strongly renormalizable, if the cut-off can be taken to infinity, whereas it is weakly renormalizable, if it is impossible to take the cut-off to infinity. A trivial theory is any theory for which the cut-off cannot be taken to infinity without forcing all interactions to zero. A trivial theory can be weakly renormalizable or non-renormalizable (or perhaps both in different regions of bare parameter space).

Possible examples of some of these classes are QCD as a strongly renormalizable theory and ϕ^4 as a weakly renormalizable theory. Where should we place QED in this classification?

In sect. 7 we have seen that the cut-off cannot be pushed to arbitrarily high energies for any finite value of e_R. As a result, QED is trivial and can at most be regarded as a valid theory up to some finite energy scale. We now want to look for lines of constant physics. This means, one needs to compare the flow of different dimensionless quantities.

We have already shown the lines of constant e_R. We now compute the ratio m_R/m_{PS} on our grid of points and interpolate the results to find the lines of constant mass ratios. For the interpolation in β and m we have used the formulae $\ln(m_R/m_{PS}) = a + b\beta$ and $\ln(m_R/m_{PS}) = c + d \ln m$, respectively. In fig. 23 these lines are compared with the lines of constant e_R. The two flows are certainly different. The trajectories of constant m_R/m_{PS} flow into the critical point, in contrast to the lines of constant e_R, which end on the first order critical line. The

inconsistency is most striking for $\beta < \beta_c$, where the e_R trajectories move in the direction of lower β (in accord with a positive β function), while the mass ratio trajectories move in the direction of larger β (as one would obtain from a negative β function). The effect does not seem to go away as one approaches the critical point, showing that it is not a lattice artifact, which would vanish as a power of the inverse of the correlation length. The lowest value of π/m_R in this figure is ≈ 2.5 (in the upper left corner), whereas the largest value is ≈ 22 (in the opposite corner). See also fig. 18 for the line $\pi/m_R = 5$. The fine structure constant α_R varies from 0.22 (lower right corner) to 0.44 (upper left corner).

Having updated the flow diagram from ref. [2], we now present some new flow diagrams calculated from the masses of the composite states found in sect. 8. We have computed the ratios m_{PS}/m_S and m_R/m_S. The interpolation was done using the same formulae as we used for the ratio m_R/m_{PS}. The lines of constant m_{PS}/m_S are shown in fig. 24. They seem to flow into the critical point. The ratio goes to one, as one approaches the second order critical line ($\beta > \beta_c$, $m = 0$), where chiral symmetry is restored. For comparison, we have plotted in fig. 25 the mean field result. There is qualitative agreement between the two figures. It is apparent that the quality of the data (in particular for m_S) needs to be improved.

The lines of constant m_R/m_S are plotted in fig. 26. This flow diagram is obviously different from those of the other mass ratios. The largest and smallest mass ratios in this plot are 0.6 and 0.3, respectively. It is interesting to note that the curves of constant fermion-antifermion scattering in the pseudoscalar channel found from the Schwinger-Dyson equations in ref. [14] look the same as the m_R/m_{PS} plot. We would expect the corresponding scalar scattering amplitude to reproduce the flow of m_R/m_S. Where we have results, the corresponding flows are indeed similar, but the Schwinger-Dyson curves extend to much smaller masses. This comparison leads us to expect that the curves of low mass ratio ($m_R/m_S \lesssim 0.4$) will all end in the critical point, whereas those of high mass ratios ($m_R/m_S \gtrsim 0.4$) will end on the first order critical line. We again find that different dimensionless quantities flow along different trajectories.

Our statements about the non-renormalizability of QED given in our previous paper [2] have been strengthened by the calculation of more quantities. In particular, by comparing figs. 23, 24 and 26 we can see non-renormalizability (i.e. the non-existence of lines of constant physics) in the matter sector, showing that this is not merely an effect of the photon.

We conclude that QED is non-renormalizable throughout the parameter region we have investigated, although it must become weakly renormalizable for small

enough α_R, and we see hints of this near our smallest α_R values ($\alpha_R \lesssim 0.22$). Non-renormalizability shows up long before the cut-off reaches its maximal value.

10 Anomalous dimensions and critical exponents

Though the photon decouples at the critical point, the matter sector of the theory may still interact through exchange of the Goldstone boson and via induced couplings, such as the four-fermi coupling. It is important now to find out, whether this is the case. One way would be by computing the appropriate renormalized couplings. This has not been done yet. Another source of information are the critical exponents. The drawback here is that it is difficult to determine the critical exponents accurately by numerical methods. A further quantity of interest is the anomalous dimension of the operator $\bar{\chi}\chi$. In mean field theory $\bar{\chi}\chi$ is treated as a quasi-free, elementary scalar field of dimension one. If this ansatz proves to be correct, it has far-reaching consequences.

The critical exponents δ, $\dot{\beta}$ (in order to avoid confusion of β and the critical exponent named by the same letter, we have called the latter $\dot{\beta}$), ν and γ are defined by

$$\delta = \left[\frac{\partial \ln\langle\bar{\chi}\chi\rangle}{\partial \ln m}\right]^{-1}\Bigg|_{\beta=\beta_c}, \tag{10.1}$$

$$\dot{\beta} = \frac{\partial \ln\langle\bar{\chi}\chi\rangle}{\partial \ln(\beta_c-\beta)}\Bigg|_{\beta\nearrow\beta_c, m=0}, \tag{10.2}$$

$$\nu = \frac{\partial \ln m_R}{\partial \ln(\beta_c-\beta)}\Bigg|_{\beta\nearrow\beta_c, m=0}, \tag{10.3}$$

$$\gamma = -\frac{\partial \ln\chi_m}{\partial \ln(\beta_c-\beta)}\Bigg|_{\beta\nearrow\beta_c}, \quad \chi_m = \frac{\partial\langle\bar{\chi}\chi\rangle}{\partial m}\Bigg|_{m=0}. \tag{10.4}$$

They are related by the scaling relations [23,40]

$$\dot{\beta}(\delta-1)=\gamma, \quad \dot{\beta}(\delta+1)=4\nu, \tag{10.5}$$

so that only two of them are independent. These relations are proven for a certain class of models and are believed to have a wider range of applicability. The

equation of state (3.3) yields the critical exponents $\delta = 3$, $\dot{\beta} = 1/2$ and $\gamma = 1$, in agreement with the first scaling relation. The second scaling relation gives, furthermore, $\nu = 1/2$. These values are referred to as mean field critical exponents. An independent information about the critical exponents comes from the relationship (5.15) between $\langle\bar{\chi}\chi\rangle$ and m_R for small m_R. It implies $\dot{\beta} = \nu$, which gives $\delta = 3$, owing to the second scaling relation. This agrees with the mean field formula we used before. It should be noted that there are several length scales in the theory (e.g. m_R and m_S), which all can be used to define a correlation length and the exponent ν. As long as they scale together as one approaches the critical point along the first order critical line, it does, however, not matter which length scale we take.

The critical exponents are interrelated with the anomalous dimensions of m and $\bar{\chi}\chi$, γ_m and $\gamma_{\bar{\chi}\chi}$, which we will discuss now. The discussion will follow ref. [24].

Let us consider mass renormalization first. We write

$$m_R = Z_m m. \tag{10.6}$$

Then γ_m is defined by (remember that $1/m_R$ acts as the cut-off)

$$\gamma_m = -\frac{\partial \ln Z_m}{\partial \ln m_R}\Bigg|_{\beta \text{ fixed}} \tag{10.7}$$

$$= \frac{\partial \ln m}{\partial \ln m_R}\Bigg|_{\beta \text{ fixed}} - 1. \tag{10.8}$$

We are primarily interested in the anomalous dimension at $\beta = \beta_c$. From eqs. (5.15) and (10.1) it follows that at $\beta = \beta_c$

$$\gamma_m = \delta - 1. \tag{10.9}$$

Our result $\delta = 3$ gives the anomalous dimension $\gamma_m = 2$. We call γ_m the renormalized anomalous dimension to distinguish it from the bare one

$$\gamma_m^0 = -\frac{\partial \ln Z_m}{\partial \ln m_R}\Bigg|_{\text{constant physics}} \tag{10.10}$$

$$= \frac{\partial \ln m}{\partial \ln m_R}\Bigg|_{\text{constant physics}} - 1. \tag{10.11}$$

There are ambiguities in this definition (because the theory is not renormalizable in the critical region). Here, in distinction to ν, it matters whether one keeps e_R or (e.g.) m_{PS}/m_S fixed. For the latter choice eqs. (3.3), (5.15), (8.5) and (8.6)

give $\gamma_m^0 = 2$. (The same sort of ambiguities are present in defining renormalized and bare β functions.)

Let us now consider renormalization of the composite operator $\bar{\chi}\chi$. We write

$$\bar{\chi}\chi_R = Z_{\bar{\chi}\chi}\bar{\chi}\chi + Z_1 \mathbf{1}. \tag{10.12}$$

This includes mixing with the 1 operator, which is the only mixing expected from perturbation theory. The anomalous dimension $\gamma_{\bar{\chi}\chi}$ is given by

$$\gamma_{\bar{\chi}\chi} = -\left.\frac{\partial \ln Z_{\bar{\chi}\chi}}{\partial \ln m_R}\right|_{\beta \text{ fixed}}. \tag{10.13}$$

Because the operators $\bar{\chi}\chi$ and 1 transform differently under chiral rotations, one would expect Z_1 to vanish like m. The different scaling laws for bare and renormalized masses at $\beta = \beta_c$ (c.f. eq. (5.17)) then lead us to expect that the operator mixing can be ignored. Thus we have

$$\gamma_{\bar{\chi}\chi} = \left.\frac{\partial \ln\langle\bar{\chi}\chi\rangle}{\partial \ln m_R}\right|_{\beta \text{ fixed}} - 3, \tag{10.14}$$

where the -3 in eq. (10.14) assumes that $\beta = \beta_c$ is a line of constant $\langle\bar{\chi}\chi_R\rangle/m_R^3$ in the limit $m_R \to 0$. This hypothesis has to be checked, and we plan to return to this in a future publication [41]. From eq. (5.15) it follows that

$$\gamma_{\bar{\chi}\chi} = -2. \tag{10.15}$$

Since $m\bar{\chi}\chi$ is a renormalization group invariant quantity (when considered in connected Green's functions, which is precisely what concerns us here), we have $\gamma_m + \gamma_{\bar{\chi}\chi} = 0$. Thus, we find $\gamma_m = 2$, and hence from eq. (10.9) we obtain $\delta = 3$. Note that this result was obtained without taking recourse to the equation of state. So, we have a second, independent hint that $\delta = 3$. Equation (10.15) means that the composite operator $\bar{\chi}\chi$ has dimension one like an elementary scalar field.

It should be noted that the above results are only correct at $\beta = \beta_c$. For $\beta > \beta_c$ we find from the equation of state (3.3) and eq. (5.15) that $m_R \propto m$ as $m \to 0$, so that $\gamma_m = 0$ on the second order line. For $\beta < \beta_c$ the renormalized fermion mass goes to a finite value as $m \to 0$, so that $\gamma_m = \infty$ on the first order line. For a direct evaluation of γ_m, which supports this result, see ref. [42]. It is worth pointing out that the bare γ function we defined in eq. (10.10) is much smoother.

Summarizing, it may be said that all our results point to mean field critical exponents. This suggests that the matter sector of the theory is also trivial. In

accord with this picture, we have also concluded that the composite operator $\bar{\chi}\chi$ has dimension one. This result leads us to expect, for example, that the four-fermi interaction becomes a relevant operator. Since it is dynamically generated in any case, it should be included in the calculation right from the start. In this light we have only explored a single point of a multi-dimensional critical surface. So, it might still be possible to find a non-trivial continuum limit in a larger space of parameters.

11 Discussion

We have made a comprehensive investigation of non-compact lattice QED. Because we are interested in chiral symmetry properties, we used staggered fermions. Before one can develop a consistent picture of QED at strong coupling, one has to look at the problem from as many sides as possible. Thus, we investigated the following quantities and topics. The first item we looked at was the equation of state to find the phase diagram. To settle the question of non-confinement, we studied the potential between static particles of variable charge. We then computed the renormalized mass and charge of the fermion, in order to find the Callan-Symanzik β function. Next, we computed the masses of fermion-antifermion composite states, to address the issues of renormalizability and the effective action.

With the help of our results we have formed the following picture. There is a line of first order transitions running from $\beta = 0$ to the tricritical point at $\beta = \beta_c$, where the chiral symmetry is spontaneously broken, and a second order line thereafter. (See, e.g., fig. 3.) This phase transition is not a deconfinement-confinement phase transition. We know this from our study of the potential, which is Coulombic at all distances and for all our values of β. This suggests that the mechanism of chiral symmetry breaking is not like that of QCD, where it is closely associated with confinement, but more like that of the Nambu–Jona-Lasinio model [25], where there is chiral symmetry breaking without confinement.

The lines of constant e_R, as shown in fig. 18, tend to the first order critical line. We saw that the behavior of the renormalized charge can be well described by one-loop renormalized perturbation theory. In particular, we found a positive Callan-Symanzik β function and no sign of any second zero. Perturbation theory allowed us to extrapolate the data. The conclusion was that, as the correlation length goes to infinity, the renormalized charge goes to zero. Thus, the theory is trivial. When comparing flows of different physical quantities, we see that the flow

lines cross, showing that the theory is not even renormalizable in the parameter range we have studied. When $\alpha_R = 1/137$ the bounds in eq. (7.8) are, however, so large that there is no contradiction with the phenomenal success of QED. However, $\alpha_R \gtrsim 1/50$ would lead to inconsistencies within the context of the standard model. This could be the reason why the fine-structure constant is so small.

Coleman and Weinberg were led by their work on scalar QED [43] to conclude that 'nature abhors massless particles with long-range interactions between them', and they speculated that a symmetry would break in such a way that this situation is avoided. They then noted that they did not have the tools to investigate spinor QED. Our calculations shed light on this question and indicate that indeed massless QED does not exist. On the first order line (i.e. in the broken phase) the mechanism is basically as Colemen and Weinberg envisioned, but on the second order line nature avoids this 'abhorrent' situation by a different mechanism, namely the vanishing of the renormalized charge.

Furthermore, we have been able to relate the fermion-antifermion composite states to the chiral condensate by means of an effective action. The effective action we used is that of a linear σ model. The coupling constant of this model goes logarithmically to zero just like e_R^3. This is consistent with our belief that QED is trivial. (It would be interesting to compute the coupling constants in that action numerically.) The success of an effective action that treats the pseudoscalars and scalars as point-like suggests that the states we see are small, with the size of order the cut-off. This is to be contrasted with the size of a conventional positronium state, which should go to infinity with the correlation length as one approaches the critical point.

The critical exponents we see are the same as in the Nambu–Jona-Lasinio model, and we have noted many qualitative similarities. For example, the gap equation of the Nambu–Jona-Lasinio model leads to qualitatively the same equation of state [10,36] as derived from the effective action [1]. This could mean that QED and the Nambu–Jona-Lasinio model are in the same universality class.

One possibility, that should be mentioned, is that, by introduction of additional interactions, QED could be made into a weakly renormalizable theory. This is possible, because if relevant operators are left out of a renormalizable (or weakly renormalizable) Lagrangian, the remaining theory will exhibit no curves of constant physics, but instead look like lattice QED, with each point in the space of bare parameters having unique physics. What other Lagrangian terms could be relevant? Many approximations to strongly coupled QED suggest that renormalization generates a chirally invariant four-fermi interaction [44,14,2]. If such term

is generated by changing the cut-off, it must be a relevant operator when added to the strongly coupled QED Lagrangian. Our indications of a large anomalous dimension for $\bar{\chi}\chi$ also give a hint that four-fermi interactions could be relevant.

After all this time QED still has surprises to offer and merits further studies.

Acknowledgements

This work was supported in part by the Deutsche Forschungsgemeinschaft. Most of the numerical computations were performed on the Cray Y-MP at the HLRZ. The $8^3 \cdot 16$ configurations were generated on the VP 100 at the RHRK, Kaiserslautern. We wish to thank all these institutions for their support. We are particularly indebted to E. Laermann for his collaboration in an earlier stage of this work and for his help in writing the code for the hybrid Monte Carlo algorithm. Thanks are also due to U.-J. Wiese for discussions on the problem of charge on a periodic lattice.

Appendices

A Calculating the masses of charged particles

An important part of this paper (and of our previous paper [2]) is the calculation of the renormalized mass of the fermion. In this appendix we show that, although the fermion propagator is of course gauge dependent, the renormalized fermion mass takes the same value in all the covariant gauges (e.g. the Feynman gauge, Landau gauge, etc.).

In non-compact QED the gauge can be fixed by adding a gauge fixing term to the action, exactly as is done in the continuum. The gauge fixing term is

$$S_{GF} = \frac{\beta}{2\lambda} \sum_x \left(\sum_\mu \bar{\Delta}_\mu A_\mu(x) \right)^2, \tag{A.1}$$

where $\bar{\Delta}_\mu$ is the backward lattice derivative. The Landau gauge is given by the case $\lambda = 0$. The action $S_G + S_F + S_{GF}$ is completely local and respects all lattice symmetries, including time translation, and so has a transfer matrix. We have also checked that S_{GF} satisfies reflection positivity.

As is usual [38], we define the charge of an operator by its transformation properties under gauge transformations θ: operators unaffected by the transformation neither create nor annihilate charge, those that acquire a factor $e^{iq\theta}$ create q units of charge. This charge definition leads to the current of eq. (6.6), which by Noether's theorem is conserved. The corresponding charge operator is given by summing the charge density j_4 over a time slice:

$$\begin{aligned} Q(t) &= \sum_{\vec{x}} j_4(\vec{x}, t) \\ &= \sum_{\vec{x}} (-1)^{x_1+x_2+x_3} \frac{i}{2} \left[\bar{\chi}(\vec{x}, t) e^{iA_4(\vec{x},t)} \chi(\vec{x}, t+1) + \bar{\chi}(\vec{x}, t+1) e^{-iA_4(\vec{x},t)} \chi(\vec{x}, t) \right]. \end{aligned} \tag{A.2}$$

The charge operator Q is gauge invariant. This operator labels every eigenstate of the transfer matrix with a charge, and it divides the spectrum into superselection sectors. This charge operator works on any lattice that admits a global gauge transformation, which includes our finite lattices with periodic boundary conditions on the gauge fields.

We will now calculate how a propagator changes when we go from one covariant gauge to another.

On a lattice with V sites there are $4V$ A_μ fields, so that the A_μ field part of the functional integral is a $4V$ dimensional integral: We can divide the integration into two parts: there is a $3V + 1$ dimensional integral over physical modes and a $V - 1$ dimensional integral over pure gauge modes. We can see this mode-counting most easily in momentum space. The $V - 1$ pure gauge modes are the longitudinal photons, those that are the (lattice) gradient of some function, one for each non-zero momentum, and the $3V+1$ physical modes are the four constant background fields (momentum zero) and the three transverse photons (those that satisfy the Landau gauge condition eq. (5.1)) for each non-zero momentum. When we make this two part division, the functional integral for the partition function factorizes, because S_G and S_F depend only on the physical modes A_{phys} (that is what gauge symmetry means), while S_{GF} depends only on the pure gauge modes A_{gauge}, because it is zero for any field that satisfies the Landau condition. Thus we can write

$$Z = \int \mathcal{D}[A_{phys}] \, \mathrm{Det}(M + m1) \exp(-S_G) \int \mathcal{D}[A_{gauge}] \exp(-S_{GF}). \tag{A.3}$$

The first integral is very complicated, and has to be done by a Monte Carlo algorithm, but the second integral is Gaussian and can be done analytically. This allows us to find the λ dependence of propagators and other gauge dependent quantities. In the Landau gauge $\exp(-S_{GF})$ acts as a δ function, forcing all the gauge modes to zero, and so forcing all configurations to satisfy the Landau condition exactly. But in the other covariant gauges every configuration of the gauge field can occur. We can label any configuration by giving the Landau configuration it is equivalent to and the gauge transformation $\theta(x)$ needed to make it satisfy the Landau condition. The probability that a configuration occurs (relative to the equivalent Landau configuration) is simply $\exp(-S_{GF})$ for the gauge fields generated by θ. Consider a gauge transformation that multiplies an operator of charge q by the factor $e^{iq\theta(x)}$, and express $\theta(x)$ in terms of its Fourier transform

$$\theta(x) = a_0 + \sum_{k \neq 0} [a_k \cos kx + b_k \sin kx]. \tag{A.4}$$

The gauge field corresponding to θ is $\Delta_\mu \theta(x)$ and has the action

$$S_{GF}(\Delta_\mu \theta(x)) = \sum_{k \neq 0} \frac{1}{2}(a_k^2 + b_k^2) \left[\frac{2\beta V}{\lambda} (4 - \sum_\mu \cos k_\mu)^2 \right]. \tag{A.5}$$

Because we can do the integral over pure gauge modes, it is possible to write down a relationship between a propagator in the Landau gauge (C_L) and that in

any other covariant gauge (C_λ):

$$\begin{aligned} C_\lambda(x_2-x_1) &= \frac{\int \mathcal{D}\theta \exp(iq(\theta(x_2)-\theta(x_1)))\exp(-S_{GF}(\Delta_\mu\theta))}{\int \mathcal{D}\theta \exp(-S_{GF}(\Delta_\mu\theta))}\, C_L(x_2-x_1) \\ &= \exp\left[-\frac{\lambda q^2}{2\beta V}\sum_{k\neq 0}\frac{1-\cos k(x_2-x_1)}{(4-\sum_\mu \cos k_\mu)^2}\right]\, C_L(x_2-x_1) \\ &\xrightarrow{V\to\infty} \exp\left[-\frac{\lambda q^2}{2\beta}\int_{-\pi}^{\pi}\frac{d^4k}{(2\pi)^4}\frac{1-\cos k(x_2-x_1)}{(4-\sum_\mu \cos k_\mu)^2}\right]\, C_L(x_2-x_1) \\ &\equiv F_\lambda(x_2-x_1)\, C_L(x_2-x_1). \end{aligned} \tag{A.6}$$

The integral in the above equation behaves logarithmically when $(x_2-x_1)^2$ is large, so that the factor F_λ behaves like a power of x_2-x_1 at distances large compared with the lattice spacing. Therefore, the mass extracted from the exponential fall-off of the propagators C_L and C_λ will be identical. We can also see that the Landau gauge is the best of the covariant gauges, in the sense that in all the other gauges the propagator will be smaller, because the factor F_λ is always less than one.

In conclusion, it should be pointed out that the results of this appendix depend heavily on the fact that the theory we are simulating is abelian and non-compact. The complications of gauge fixing in non-abelian theories are well known, but even fixing a compact version of the $U(1)$ Landau gauge is a delicate matter [45].

B An alternative calculation of the fermion mass

As already pointed out, the fermion propagator is not gauge independent, though its mass is. (See appendix A.) This has caused us some unease. So, we decided to make an independent determination of m_R. We shall now consider a widely separated fermion-antifermion pair for our second calculation.

In order to have a gauge-invariant description of the fermion-antifermion pair, one could introduce the appropriate parallel transporters between fermion and antifermion. To avoid the fluctuation of a large gauge field string, we have chosen to fix the gauge. However, this time we have chosen the Coulomb gauge. The Coulomb gauge condition

$$\sum_{i=1}^{3}\bar{\Delta}_i A_i(x) = 0 \tag{B.1}$$

does neither eliminate gauge transformations depending only on the time nor the

invariance (5.2). However, by studying the correlation function of the operator

$$\mathcal{O}(t) = \sum_{\vec{x}} r(\vec{x},t)\overline{\chi}(\vec{x},t)\chi(\vec{x}+2\vec{d},t) \tag{B.2}$$

with its (lattice) charge conjugate

$$\overline{\mathcal{O}}(t) = \sum_{\vec{x}} r(\vec{x},t)\overline{\chi}(\vec{x}+2\vec{d},t)\chi(\vec{x},t) \tag{B.3}$$

for fixed (t independent) separation $2\vec{d}$ (all components even), we only have to deal with expectation values of operators, which are invariant under (5.2). The factor $r(\vec{x},t)$ denotes the sign factor of local 'mesonic' operators [5] (see ,e.g., ref. [46]).

If $L_1 = L_2 = L_3$ is a multiple of four (as is the case for our lattices), it is particularly advantageous to choose $2d_i = L_i/2$: first, (Coulomb) interaction effects are minimized and, secondly, $\mathcal{O}(t)$ transforms like the composite operator

$$\sum_{\vec{x}} r(\vec{x},t)\overline{\chi}(\vec{x},t)\chi(\vec{x},t) \tag{B.4}$$

under the lattice symmetry group (except for charge conjugation), so that the group theoretical analysis of the local 'mesonic' operators [46] applies.

We have calculated (the connected part of) $\langle\mathcal{O}(t)\overline{\mathcal{O}}(0)\rangle$ with $2d_i = 6$ averaged over blocks of 20 successive configurations on our 12^4 lattices for $m = 0.04$ and $\beta = 0.17, 0.22$. Unfortunately, the results are rather noisy. Nevertheless, we performed the following two types of fits. First, we employed the standard parametrization (8.1) of meson correlation functions. Secondly, we computed the expectation value of $\mathcal{O}(t)\overline{\mathcal{O}}(0)$ for free fermions in the presence of a constant background field B_μ and used the resulting expression as a fit function. For even times, $2t$, one finds

$$\begin{aligned} &4(L_1L_2L_3)^{-1}\sum_{\vec{p}}\sinh^{-2}(2\mu_0(\vec{p}))\left(\cosh^2(\tfrac{1}{2}L_4\mu_0(\vec{p})) - \sin^2(\tfrac{1}{2}L_4B_4)\right)^{-2} \\ &\quad\times\Big\{\sin^2(\tfrac{1}{2}L_4B_4)\sinh^2(\tfrac{1}{2}L_4\mu_0(\vec{p}))\cosh^2(\mu_0(\vec{p})(\tfrac{1}{2}L_4-2t)) \\ &\qquad+\cos^2(\tfrac{1}{2}L_4B_4)\cosh^2(\tfrac{1}{2}L_4\mu_0(\vec{p}))\sinh^2(\mu_0(\vec{p})(\tfrac{1}{2}L_4-2t))\Big\} \\ &\quad\times\left\{\tilde{s}\sum_{j=1}^{3}\sin^2(p_j+B_j)+m_R^2\right\}, \end{aligned} \tag{B.5}$$

[5] Averaging the correlation functions over directions leads to the factors $s(\vec{x},t)$ given in eq. (8.2).

whereas for odd times, $2t+1$, one obtains

$$(L_1L_2L_3)^{-1}\sum_{\vec{p}}\cosh^{-2}(2\mu_0(\vec{p}))\left(\cosh^2(\tfrac{1}{2}L_4\mu_0(\vec{p}))-\sin^2(\tfrac{1}{2}L_4B_4)\right)^{-2}$$
$$\times\left\{\sin^2(\tfrac{1}{2}L_4B_4)\sinh^2(\tfrac{1}{2}L_4\mu_0(\vec{p}))\sinh^2(\mu_0(\vec{p})(\tfrac{1}{2}L_4-2t-1))\right. \tag{B.6}$$
$$\left.+\cos^2(\tfrac{1}{2}L_4B_4)\cosh^2(\tfrac{1}{2}L_4\mu_0(\vec{p}))\cosh^2(\mu_0(\vec{p})(\tfrac{1}{2}L_4-2t-1))\right\}.$$

Here

$$\sinh(\mu_0(\vec{p}))=\sqrt{m_R^2+\sum_{j=1}^{3}\sin^2(p_j+B_j)}, \tag{B.7}$$

and the coefficient $\tilde{s}$ depends on the sign factor $r(\vec{x},t)$ chosen in $\mathcal{O}(t)$. If $\mathcal{O}(t)$ is such that the correlation function of the corresponding local operator (B.4) is the PS-$\bar{S}$ correlation function, one has $\tilde{s}=1$. In the case of the $\widetilde{PS}$-S correlation function $\tilde{s}=-1$. For the V-T ($\widetilde{V}$-A) correlation function one gets, after averaging over the three space directions, $\tilde{s}=1/3$ ($\tilde{s}=-1/3$).

Taking for the background potential the value extracted from the configurations under consideration, we ended up in this case with two free parameters for each choice of $r(\vec{x},t)$, namely the fermion mass m_R and an amplitude.

The rather large errors of the data prevent any definitive conclusion. Nevertheless, we can make the following statements. The first type of fit leads to relatively large masses ($>2m_R$). This is probably caused by the fact that, due to the fixed fermion-antifermion distance, states with various relative momenta contribute to the correlation function. The second type of fit, using the fermion propagator in a background field, leads to mass values, which are comparable with those given in table 3. However, it does not allow for a precise determination of m_R: even rather large changes of the mass increase the χ^2 only slightly, if the amplitude is modified appropriately. Therefore, the method for the calculation of m_R described in sect. 5 is superior. Nevertheless, we see (at least qualitatively) that the propagation of a fermion-antifermion pair created at a distance of $6\sqrt{3}$ lattice spacings can be described by the propagation of a free pair of a fermion and antifermion of mass m_R. This finding lends further support to our method of extracting the renormalized fermion mass from the fermion propagator in Landau gauge.

C Perturbation theory in the presence of background fields

In perturbation theory we make an expansion about the large β (or β_R) limit of our theory. Before doing this, we have to consider the theory at $\beta=\infty$. At infinite β only those A field configurations, for which all plaquettes are zero, can contribute to the functional integral. The pure gauge modes survive in this limit, but they are irrelevant for any gauge invariant quantity. There are, however, four physical modes that also survive at $\beta=\infty$. These are the constant background fields B_μ discussed in sect. 5. Although they receive no action from S_G, they are not completely free, because the fermion determinant, $\mathrm{Det}(M+m1)$, depends on B_μ. This is a finite size effect, because only those fermions, whose world lines wrap around the torus, can detect B_μ. The explicit expression for the fermion determinant is

$$\mathrm{Det}(M+m1)=\prod_k\left(m^2+\sum_\mu\sin^2(k_\mu+B_\mu)\right)^{\frac{1}{2}}. \tag{C.1}$$

The product is to run over all momenta $(-\pi,\pi]$ consistent with the boundary conditions. The determinant takes the form of a product over momentum states, because the background fields do not break translation invariance. So, the eigenvectors of M are still states of definite momentum. The effect of B_μ is simply to change the eigenvalues. When we invert the fermion matrix, we find that the effect on the fermion propagator of the background field is again to replace k_μ by $k_\mu+B_\mu$.

As an example of the results delivered by doing perturbation theory in a background, field we give the formula for the chiral condensate at $\beta=\infty$:

$$\langle\bar{\chi}\chi\rangle=\frac{\int d^4B\,\mathrm{Det}(M+m1)\sum_k m\left(m^2+\sum_\mu\sin^2(k_\mu+B_\mu)\right)^{-1}}{\int d^4B\,\mathrm{Det}(M+m1)}. \tag{C.2}$$

An interesting feature of this formula is that it does not depend on whether the fermion boundary conditions are periodic or anti-periodic. If the boundary condition in the μ direction is changed from periodic to anti-periodic (or vice versa), the distribution of B given by (C.1) shifts by π/L_μ, so that the condensate (C.2) remains unchanged. This is a completely general result (holding at all β values), a change in one of the boundary conditions is always exactly compensated by adding π/L_μ to all A fields in that direction [47]. We have used anti-periodic boundary conditions in the time direction and periodic in the space directions, but all the

gauge invariant quantities we present in this paper would be unchanged if we had taken another combination of fermion boundary conditions.

When we calculate the one-loop polarization correction in section 6, we also use a weighted average over backgrounds similar to (C.2). Both, for the chiral condensate and the polarization tensor, we find that results on a 12^4 lattice scarcely differ from those on an infinite lattice, and even the difference between perturbation theory on an infinite and on an 8^4 lattice is minor. Thus, the influence of the background field on these quantities is negligible.

References

[1] M. Göckeler, R. Horsley, E. Laermann, P. Rakow, G. Schierholz, R. Sommer and U.-J. Wiese, Nucl. Phys. **B334** (1990) 527

[2] M. Göckeler, R. Horsley, E. Laermann, P. Rakow, G. Schierholz, R. Sommer and U.-J. Wiese, Phys. Lett. **251B** (1990) 567; Erratum, *ibid.* **256B** (1991) 562

[3] K. Johnson, M. Baker and R. Willey, Phys. Rev. **136** (1964) 111; *ibid.* **163** (1967) 1699;
S. Adler and W. A. Bardeen, Phys. Rev. **D4** (1971) 3045;
S. Adler, Phys. Rev. **D5** (1972) 3021

[4] D. A. Kirzhnits and A. D. Linde, Phys. Lett. **73B** (1978) 323;
P. Olesen, Phys. Lett. **73B** (1978) 327;
N. V. Krasnikov, Phys. Lett. **126B** (1983) 483;
For historical reviews see:
V. B. Berestetskii, Sov. Phys. Usp. **19** (1976) 934;
S. Aramaki, Nagoya preprint DPNU-89-20 (1989)

[5] B. Holdom, Phys. Lett. **150B** (1985) 301; *ibid.* **198B** (1987) 535;
K. Yamawaki, M. Bando and K. Matumoto, Phys. Rev. Lett. **56** (1986) 1335;
T. Akiba and T. Yanagida, Phys. Lett. **169B** (1986) 432;
T. Appelquist and L. C. R. Wijewardhana, Phys. Rev. **D36** (1987) 563

[6] Y. Nambu, in *1988 International Workshop on New Trends in Strong Coupling Gauge Theories*, p. 3, eds. M. Bando, T. Muta and K. Yamawaki (World Scientific, Singapore, 1989); in *Proceedings of 1989 Workshop on Dynamical Symmetry Breaking*, p. 1, eds. T. Muta and K. Yamawaki (Nagoya University, Nagoya, 1990);
V. A. Miransky, M. Tanabashi and K. Yamawaki, Phys. Lett. **221B** (1989) 177; Mod. Phys. Lett. **A4** (1989) 1043;
W. A. Bardeen, C. T. Hill and M. Lindner, Phys. Rev. **D41** (1990) 1647;
W. J. Marciano, Phys. Rev. Lett. **62** (1989) 2793;
M. Suzuki, Phys. Rev. **D41** (1990) 3457; Mod. Phys. Lett. **A5** (1990) 1205

[7] V. A. Miransky, Nuovo Cim. **90A** (1985) 149; Sov. Phys. JETP **61** (1985) 905;
P. I. Fomin, V. P. Gusynin, V. A. Miransky and Yu. A. Sitenko, Riv. Nuovo Cim. **6** (1983) 1

[8] J. B. Kogut, E. Dagotto and A. Kocic, Phys. Rev. Lett. **60** (1988) 772; Nucl. Phys. **B317** (1989) 253; *ibid.* **B317** (1989) 271

[9] S. P. Booth, R. D. Kenway and B. J. Pendleton, Phys. Lett. **228B** (1989) 115

[10] A. M. Horowitz, Phys. Lett. **244B** (1990) 306

[11] K.-I. Kondo, in *1990 International Workshop on Strong Coupling Gauge Theories and Beyond*, p. 233, eds. T. Muta and K. Yamawaki (World Scientific, Singapore, 1991)

[12] P. E. L. Rakow, in *1990 International Workshop on Strong Coupling Gauge Theories and Beyond*, p. 249, eds. T. Muta and K. Yamawaki (World Scientific, Singapore, 1991)

[13] S. W. de Souza and R. D. Kenway, Phys. Lett. **248B** (1990) 423; Nucl. Phys. **B354** (1991) 39

[14] P. E. L. Rakow, Nucl. Phys. **B356** (1991) 27

[15] D. Brydges and E. Seiler, J. Stat. Phys. **42** (1986) 405

[16] J. B. Kogut and E. Dagotto, Phys. Rev. Lett. **59** (1987) 617

[17] H. C. Hege and A. Nakamura, Nucl. Phys. **B** (Proc. Suppl.) **9** (1989) 235

[18] M. Okawa, Phys. Rev. Lett. **62** (1989) 1224

[19] S. Duane, A. D. Kennedy, B. J. Pendleton and D. Roweth, Phys. Lett. **195B** (1987) 216

[20] K. Bitar, A. D. Kennedy, R. Horsley, S. Meyer and P. Rossi, Nucl. Phys. **B313** (1989) 348

[21] T. Jolicoeur and A. Morel, Nucl. Phys. **B262** (1985) 627

[22] J. Gasser and H. Leutwyler, Phys. Lett. **188B** (1987) 477

[23] E. Brezin, J. C. Le Guillou and J. Zinn-Justin, in *Phase Transitions and Critical Phenomena*, Vol. 6, p. 125, eds. C. Domb and M. S. Green (Academic Press, London, 1976)

[24] G. Schierholz, Nucl. Phys. **B** (Proc. Suppl.) **20** (1991) 623

[25] Y. Nambu and G. Jona-Lasinio, Phys. Rev. **122** (1961) 345

[26] L. A. Griffiths, C. Michael and P. E. L. Rakow, Phys. Lett. **129B** (1983) 351; R. Sommer, Nucl. Phys. **B306** (1988) 181

[27] S. J. Hands, J. B. Kogut, R. Renken, A. Kocic, D. K. Sinclair and K. C. Wang, Phys. Lett. **261B** (1991) 294

[28] M. Göckeler, Nucl. Phys. **B** (Proc. Suppl.) **20** (1991) 642

[29] A. Nakamura and R. Sinclair, Phys. Lett. **243B** (1990) 396

[30] F. Gliozzi, Nucl. Phys. **B204** (1982) 419;
H. Kluberg-Stern, A. Morel, O. Napoly and B. Petersson, Nucl. Phys. **B220** (1983) 447

[31] T. Jolicoeur, A. Morel and B. Petersson, Nucl. Phys. **B274** (1986) 225

[32] Y. Nambu, in *Proceedings of 1989 Workshop on Dynamical Symmetry Breaking*, p. 1, eds. T. Muta and K. Yamawaki (Nagoya University, Nagoya, 1990)

[33] R. Horsley et al., Nucl. Phys. **B** (Proc. Suppl.) **20** (1991) 639

[34] M. Lüscher, Nucl. Phys. **B341** (1990) 341

[35] U. Heller and F. Karsch, Nucl. Phys. **B258** (1985) 29

[36] A. Horowitz, Phys. Rev. **D43** (1991) 43

[37] A. Horowitz, Nucl. Phys. **B** (Proc. Suppl.) **20** (1991) 635

[38] J. D. Bjorken and S. D. Drell, *Relativistic Quantum Fields* (McGraw-Hill, New York, 1965)

[39] M. Gell-Mann and M. Levy, Nuovo Cim. **16** (1960) 705

[40] D. J. Amit, *Field Theory, the Renormalization Group, and Critical Phenomena* (World Scientific, Singapore, 1984)

[41] M. Göckeler, R. Horsley, P. Rakow and G. Schierholz, in preparation

[42] G. Schierholz, in *1990 International Workshop on Strong Coupling Gauge Theories and Beyond*, p. 279, eds. T. Muta and K. Yamawaki (World Scientific, Singapore, 1991)

[43] S. Coleman and E. Weinberg, Phys. Rev. **D7** (1973) 1888

[44] C. N. Leung, S. T. Love and W. A. Bardeen, Nucl. Phys. **B273** (1986) 649

[45] A. Nakamura and M. Plewnia, Phys. Lett. **255B** (1991) 274

[46] M.F.L. Golterman, Nucl. Phys. **B273** (1986) 663

[47] P. Rossi and J. Sloan, San Diego preprint UCSD-PTH-89-10 (1989)

Table captions

Table 1:
The chiral condensate $\langle\bar{\chi}\chi\rangle$ on the 8^4, $8^3\cdot 16$ and 12^4 lattices at various values of β and m. The errors shown are purely statistical.

Table 2:
The average gauge field action per plaquette $\langle S_G\rangle/(6V\beta)$ on the 8^4, $8^3\cdot 16$ and 12^4 lattices at various values of β and m. The errors shown are purely statistical.

Table 3:
The renormalized fermion mass m_R on the 8^4, $8^3\cdot 16$ and 12^4 lattices at various values of β and m as obtained from a fit with $t_0 = 1$. The errors shown are purely statistical.

Table 4:
The renormalized charge on the 8^4 and 12^4 lattices at various values of β and m. The errors are purely statistical. Note that the errors should be compared with $\beta_R - \beta$, which is the quantity that is actually computed.

Table 5:
The mass of the Goldstone boson m_{PS} on the 8^4, $8^3\cdot 16$ and 12^4 lattices as well as the mass of the scalar particle m_S on the 12^4 lattice at various values of β and m as obtained from a fit with $t_0 = 1$. The errors shown are purely statistical.

		$\langle\bar{\chi}\chi\rangle$		
β	m	8^4	$8^3 \cdot 16$	12^4
0.16	0.16	0.4782(5)		
	0.09	0.4470(7)	0.4474(5)	
	0.04	0.4062(12)	0.4059(7)	
	0.02	0.3804(16)		
0.17	0.16			0.4577(3)
	0.09			0.4194(3)
	0.04			0.3698(7)
	0.02			0.3329(9)
0.18	0.16	0.4380(5)		0.4375(3)
	0.09	0.3907(7)	0.3918(5)	0.3910(3)
	0.04	0.3281(11)	0.3264(6)	0.3277(6)
	0.02	0.2790(18)		0.2855(8)
0.19	0.16	0.4172(5)		0.4177(2)
	0.09	0.3619(6)		0.3635(3)
	0.04	0.2850(13)		0.2892(6)
	0.02	0.2255(15)		0.2340(7)
	0.01			0.1835(13)
0.20	0.16	0.3975(5)		0.3982(2)
	0.09	0.3361(5)	0.3377(4)	0.3377(3)
	0.04	0.2483(18)	0.2477(5)	0.2514(5)
	0.02	0.1694(10)		0.1891(6)
	0.01			0.1322(10)
0.21	0.16	0.3798(4)		0.3798(2)
	0.09	0.3124(5)		0.3123(2)
	0.04			0.2197(4)
	0.02			0.1550(6)
	0.01			0.0917(6)
0.22	0.16	0.3618(5)		0.3624(2)
	0.09	0.2887(5)	0.2881(4)	0.2898(2)
	0.04	0.1808(10)	0.1845(4)	0.1917(4)
	0.02	0.1012(34)		0.1213(4)

Table 1

		$\langle S_G\rangle/(6V\beta)$		
β	m	8^4	$8^3 \cdot 16$	12^4
0.16	0.16	1.4280(8)		
	0.09	1.4018(8)	1.4005(6)	
	0.04	1.3739(11)	1.3736(6)	
	0.02	1.3617(22)		
0.17	0.16			1.3376(4)
	0.09			1.3093(5)
	0.04			1.2832(6)
	0.02			1.2669(6)
0.18	0.16	1.2583(5)		1.2577(4)
	0.09	1.2287(8)	1.2297(6)	1.2303(4)
	0.04	1.2031(9)	1.2013(6)	1.2022(6)
	0.02	1.1873(20)		1.1881(6)
0.19	0.16	1.1872(6)		1.1876(4)
	0.09	1.1589(6)		1.1610(3)
	0.04	1.1331(13)		1.1343(5)
	0.02	1.1166(11)		1.1194(5)
	0.01			1.1106(9)
0.20	0.16	1.1244(5)		1.1256(3)
	0.09	1.1000(7)	1.0990(4)	1.0997(3)
	0.04	1.0731(7)	1.0735(5)	1.0739(3)
	0.02	1.0592(6)		1.0617(4)
	0.01			1.0548(6)
0.21	0.16	1.0205(5)		1.0695(3)
	0.09	1.0466(5)		1.0455(3)
	0.04			1.0234(4)
	0.02			1.0133(4)
	0.01			1.0068(4)
0.22	0.16	1.0205(5)		1.0206(3)
	0.09	0.9972(4)	0.9970(4)	0.9978(2)
	0.04	0.9771(8)	0.9775(4)	0.9779(3)
	0.02	0.9679(6)		0.9692(3)

Table 2

		m_R		
β	m	8^4	$8^3 \cdot 16$	12^4
0.16	0.16	1.26(6)		
	0.09	1.10(6)	1.02(4)	
	0.04	0.87(11)	0.81(3)	
	0.02	0.80(4)		
0.17	0.16			1.160(8)
	0.09			0.945(5)
	0.04			0.748(6)
	0.02			0.636(7)
0.18	0.16	1.08(4)		1.047(5)
	0.09	0.80(2)	0.85(2)	0.825(4)
	0.04		0.63(1)	0.635(3)
	0.02	0.46(5)		0.512(7)
0.19	0.16	0.96(2)		0.960(5)
	0.09	0.75(1)		0.739(4)
	0.04	0.51(2)		0.537(4)
	0.02			0.404(3)
	0.01			0.302(4)
0.20	0.16	0.87(1)		0.883(4)
	0.09	0.66(1)	0.68(2)	0.663(3)
	0.04	0.44(1)	0.43(1)	0.448(3)
	0.02	0.29(1)		0.313(3)
	0.01			0.214(4)
0.21	0.16	0.79(1)		0.814(2)
	0.09	0.61(1)		0.594(2)
	0.04			0.386(2)
	0.02			0.257(2)
	0.01			0.145(3)
0.22	0.16	0.80(3)		0.754(2)
	0.09	0.54(1)	0.56(1)	0.541(2)
	0.04	0.31(1)	0.32(1)	0.323(2)
	0.02	0.18(1)		0.194(3)

Table 3

		$\beta_R = 1/e_R^2$	
β	m	8^4	12^4
0.16	0.16	0.1803(4)	
	0.09	0.1867(6)	
	0.04	0.1951(11)	
	0.02	0.1996(9)	
0.17	0.16		0.1942(1)
	0.09		0.2028(2)
	0.04		0.2141(3)
	0.02		0.2220(4)
0.18	0.16	0.2086(6)	0.2085(2)
	0.09	0.2187(8)	0.2190(2)
	0.04		0.2332(4)
	0.02	0.2471(12)	0.2455(5)
0.19	0.16	0.2230(7)	0.2224(2)
	0.09	0.2351(8)	0.2347(2)
	0.04	0.2535(14)	0.2538(3)
	0.02		0.2703(4)
	0.01		0.2901(7)
0.20	0.16	0.2358(7)	0.2359(2)
	0.09	0.2530(10)	0.2510(2)
	0.04	0.2758(11)	0.2748(3)
	0.02	0.3027(11)	0.2988(4)
	0.01		0.3241(7)
0.21	0.16		0.2502(2)
	0.09		0.2674(2)
	0.04		0.2948(3)
	0.02		0.3222(6)
	0.01		0.3618(6)
0.22	0.16	0.2628(7)	0.2641(2)
	0.09	0.2846(9)	0.2835(3)
	0.04	0.3226(12)	0.3172(4)
	0.02	0.3626(13)	0.3517(4)

Table 4

		m_{PS}			m_S
β	m	8^4	$8^3 \cdot 16$	12^4	12^4
0.16	0.16	0.941(3)			
	0.09	0.720(3)	0.723(2)		
	0.04	0.508(2)	0.501(3)		
	0.02	0.360(3)			
0.17	0.16			0.951(2)	1.96(6)
	0.09			0.736(2)	1.54(1)
	0.04			0.513(3)	1.32(5)
	0.02			0.376(3)	1.23(5)
0.18	0.16	0.961(4)		0.961(2)	1.76(5)
	0.09	0.749(8)	0.750(2)	0.751(3)	1.45(4)
	0.04	0.543(3)	0.534(3)	0.533(4)	1.20(3)
	0.02			0.397(5)	0.99(3)
0.19	0.16	0.947(3)		0.973(2)	1.63(1)
	0.09	0.768(3)		0.767(2)	1.34(2)
	0.04	0.553(3)		0.552(3)	1.03(2)
	0.02	0.447(4)		0.419(4)	0.88(2)
	0.01			0.325(9)	0.68(3)
0.20	0.16	0.990(4)		0.986(2)	1.60(4)
	0.09	0.787(5)	0.784(17)	0.783(2)	1.30(1)
	0.04	0.583(5)	0.584(4)	0.576(3)	0.96(1)
	0.02	0.498(8)		0.454(4)	0.74(1)
	0.01			0.365(8)	0.57(7)
0.21	0.16	0.996(3)		0.998(2)	1.53(1)
	0.09	0.804(4)		0.798(2)	1.25(1)
	0.04			0.595(3)	0.92(1)
	0.02			0.468(4)	0.75(1)
	0.01			0.434(7)	0.50(5)
0.22	0.16	1.014(4)		1.008(2)	1.49(1)
	0.09	0.824(5)	0.819(3)	0.814(2)	1.19(1)
	0.04	0.676(7)	0.646(4)	0.622(3)	0.87(1)
	0.02	0.613(14)		0.525(4)	0.65(1)

Table 5

Figure captions

Fig. 1:
$\langle\bar{\chi}\chi\rangle$ as a function of β. We compare the data with a fit from eq. (3.3). The symbols refer to the different masses: $m = 0.01$ ($\diamond$), 0.02 ($\bigtriangledown$), 0.04 ($\circ$), 0.09 ($\Box$) and 0.16 ($\bigtriangleup$). All errors are smaller than the symbols. The lattice sizes are $8^3 \cdot 16$ ($m = 0.04$, 0.09) and 8^4 ($m = 0.02$, 0.16) for $\beta = 0.16$ and 12^4 for $\beta = 0.17$ - 0.22. The dashed curve is the extrapolation to $m = 0$. The fit did not include the data values at $m = 0.16$. The parameters of the fit are $\beta_c = 0.186(1)$, $p = 0.61$, $\tau_1 = -0.84(1)$, $\theta_0 = 0.59(1)$ and $\theta_1 = -0.30(2)$.

Fig. 2:
Scaling plot of $(\beta_c - \beta)/\sigma^2 \ln^{p-1}|\sigma^{-1}|$ against $m \ln|\sigma^{-1}|/\sigma^3$ for $\beta_c = 0.186$ and $p = 0.61$ on the 12^4 lattice. If the critical indices have mean field values with logarithmic corrections as described by the equation of state (3.3), all data near the phase transition should lie on a universal curve.

Fig. 3:
The phase diagram. The dashed line represents the second order critical line, whereas the solid line represents the first order critical line. The solid circle marks the tricritical point.

Fig. 4:
The effective potential $V_q^{eff}(\vec{x})$ as a function of q^2 on the 12^4 lattice at $\beta = 0.17$, $m = 0.02$. The bare parameters were chosen as close as possible to the first order critical line, i.e. the phase where chiral symmetry is broken. The symbols refer to different distances: $\vec{x}$ = (1,0,0) ($\circ$), (1,1,0) ($\Box$), (1,1,1) ($\bigtriangleup$) and (6,6,6) ($\diamond$).

Fig. 5:
The potential $V_q^{eff}(\vec{x})$ as a function of $|\vec{x}|$ on the 12^4 lattice for $q = 0.3$. The bare parameters are (a) $\beta = 0.17$, $m = 0.02$ and (b) $\beta = 0.22$, $m = 0.02$. Usually, we shall show our results for these two parameter sets, representing the behavior of the theory in the two different phases. We compare the data with the Coulomb potential. The open symbols are our data. The different kind of symbols refer to

$\vec{x} = (l,0,0)$ (○), $(l,l,0)$ (□) and (l,l,l) (△) with $l = 1, 2, \ldots, 6$. The solid symbols are a fit with the lattice Coulomb potential (4.8), (4.9). The fit did not include the data points at $|\vec{x}| = 1$. The different kinds of symbols refer to the same $\vec{x}$ as the data. The parameters of the fit are (a) $e^2_{eff} = 4.35(17)$, $E_0 = 0.104(33)$ and (b) $e^2_{eff} = 2.88(7)$, $E_0 = 0.147(14)$.

Fig. 6:
The background field $\bar{A}_4$ on the 12^4 lattice at $\beta = 0.22$, $m = 0.02$ as a function of configuration number. Consecutive configurations are separated by 5 trajectories. We see jumps from $\bar{A}_4 = +\pi/12$ to $\bar{A}_4 = -\pi/12$ and back.

Fig. 7:
The real (a) and imaginary (b) part of the fermion propagator $G_{\vec{0}}(t)$ as a function of t on the 12^4 lattice at $\beta = 0.17$, $m = 0.02$ for one set of 20 configurations. The stars are our data. The lines are a fit to the data for $t_0 = 1$. Because of the properties of staggered fermions the even and odd points lie on different curves. The solid (dashed) lines refer to even (odd) t.

Fig. 8:
The same as fig. 7 but for $\beta = 0.22$, $m = 0.02$.

Fig. 9:
The chiral condensate against the renormalized fermion mass. The symbols refer to the different values of β: $\beta = 0.16$ (◆), 0.17 (▲), 0.18 (■), 0.19 (□), 0.20 (△), 0.21 (◇), 0.22 (○). The lattice sizes are $8^3 \cdot 16$ ($m = 0.04$, 0.09) and 8^4 ($m = 0.02$, 0.16) for $\beta = 0.16$ and 12^4 for $\beta = 0.17$ - 0.22. The solid symbols are for β values below β_c, while the open symbols are for β values above β_c. The dashed line is the one-loop lattice result, as given by eq. (5.14), which is included for comparison.

Fig. 10:
A sketch of $\Sigma(p)$ for soft and hard chiral symmetry breaking.

Fig. 11:
The photon-photon correlation function $1 - D(k)$, as given by eq. (6.4), as a

function of $(kL/2\pi)^2$ on the 12^4 lattice at $\beta = 0.17$, $m = 0.02$. Here $L = L_\mu = 12$.

Fig. 12:
The current-photon correlation function $1 - D(k)$, as given by eq. (6.7), on the 12^4 latttice evaluated at the smallest non-zero value of the photon momentum, $k^2 = (2\pi/12)^2$. This is plotted against R, the number of random number sets. The bare parameters are $\beta = 0.17$, $m = 0.02$.

Fig. 13:
The current-photon correlation function $1 - D(k)$ as a function of $(kL/2\pi)^2$ on the 12^4 lattice at (a) $\beta = 0.17$, $m = 0.02$ and (b) $\beta = 0.22$, $m = 0.02$. The open circles are our data. The solid circles are a fit with the one-loop lattice result. The solid diamond is the extrapolation to zero momentum and infinite volume, which gives us the renormalized charge. The error on the latter quantity is smaller than the symbol.

Fig. 14:
Polynomial fit to the current-photon correlation function $1 - D(k)$ on the 12^4 lattice at $\beta = 0.22$, $m = 0.02$. The open circles are our data. The solid line is a fourth order polynomial fit.

Fig. 15:
The potential $V_q^{cJJ}(\vec{x})$ as a function of $|\vec{x}|$ on the 12^4 lattice for $q = 0.3$. The bare parameters are $\beta = 0.17$, $m = 0.02$. We compare the data with the one loop corrected Coulomb potential, where m_R and e^2_R are taken from tables 3 and 4, respectively. The open symbols are our data. The solid symbols are the prediction of eqs. (6.17), (6.18). The meaning of the different kinds of symbols is the same as in fig. 5.

Fig. 16:
The relationship between e^2_R, e^2 and m_R. The data symbols are the same as those in fig. 9. The lattice sizes are 8^4 for $\beta = 0.16$ and 12^4 for $\beta = 0.17$ - 0.22. The solid symbols are for β values below β_c, while the open symbols are for β values above β_c. The dashed line is the prediction of the one-loop β function shifted to

fit the data point at the smallest value of m_R, which corresponds to $\beta = 0.21$, $m = 0.01$.

Fig. 17:
The Callan-Symanzik β function times $3\pi^2/2e_R^4$ (i.e. normalized to one at $m_R = 0$, $e_R = 0$) on the 12^4 lattice. The data symbols are the same as in fig. 9. This is compared with the one-loop lattice β function given by the dashed line.

Fig. 18:
The renormalization group flow in the critical region. The solid lines are lines of constant renormalized charge, where e_R^2 ranges from $e_R^2 = 2.8$ (lower right-hand corner) to $e_R^2 = 5.4$ (upper left-hand corner) in steps of 0.2. The uncertainty in the position of the flow lines is about 5 % of the spacing between lines. The dashed line corresponds to a cut-off of $\pi/m_R = 5$. The solid diamond indicates the critical point.

Fig. 19:
The correlation function $C(t)$ for the PS - $\bar{S}$ channel as a function of t on the 12^4 lattice at (a) $\beta = 0.17$, $m = 0.02$ and (b) $\beta = 0.22$, $m = 0.02$. The stars are our data. The errors are smaller than the symbols. The lines are a fit of a single PS state to the data for $t_0 = 1$.

Fig. 20:
The correlation function $C(t)$ for the $\widetilde{PS}$ - S channel as a function of t on the 12^4 lattice at $\beta = 0.22$, $m = 0.02$. The stars are our data. The errors are smaller than the symbols. The lines are a fit of a single S state to the data for $t_0 = 1$.

Fig. 21:
m_{PS}^2 as a function of $m/\sigma \ln^{0.5}|\sigma^{-1}|$ on the 12^4 lattice. The data symbols are the same as in fig. 9.

Fig. 22:
$m_S^2 - m_{PS}^2$ as a function of the right-hand side of eq. (8.8) with parameters obtained from previous fits. The data symbols are the same as in fig. 9. The solid line is

the prediction of the effective action.

Fig. 23:
The renormalization group flow in the critical region. The dotted lines are lines of constant renormalized charge already shown in fig. 18. The solid lines are lines of constant m_R/m_{PS} ranging from 0.4 (lower right-hand corner) to 2.1 (lower left-hand corner) in steps of 0.1. The uncertainty in the position of the flow lines is about 10 % for the mass-ratio lines. The solid diamond indicates the critical point.

Fig. 24:
The renormalization group flow in the critical region. The solid lines are lines of constant m_{PS}/m_S ranging from 0.35 (lower left-hand corner) to 0.85 (lower right-hand corner) in steps of 0.05. The uncertainty in the position of the flow lines is about 20 % of the spacing between the lines. The solid diamond indicates the critical point.

Fig. 25:
The renormalization group flow in the critical region as predicted by the effective action (8.3) with parameters obtained from previous fits. The solid lines are lines of constant m_{PS}/m_S ranging from 0.25 (lower left-hand corner) to 0.9 (lower right-hand corner) in steps of 0.05.

Fig. 26:
The renormalization group flow in the critical region. The solid lines are lines of constant m_R/m_S ranging from 0.6 (on the left) to 0.3 (on the right) in steps of 0.025. The solid diamond indicates the critical point.

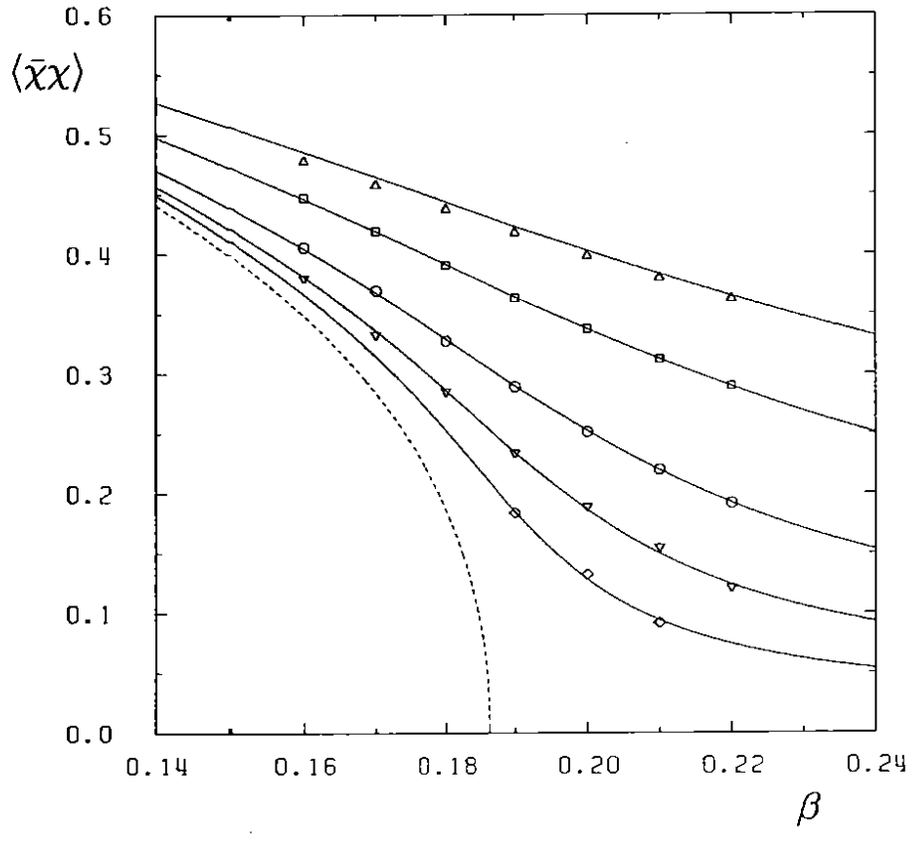

Figure 1

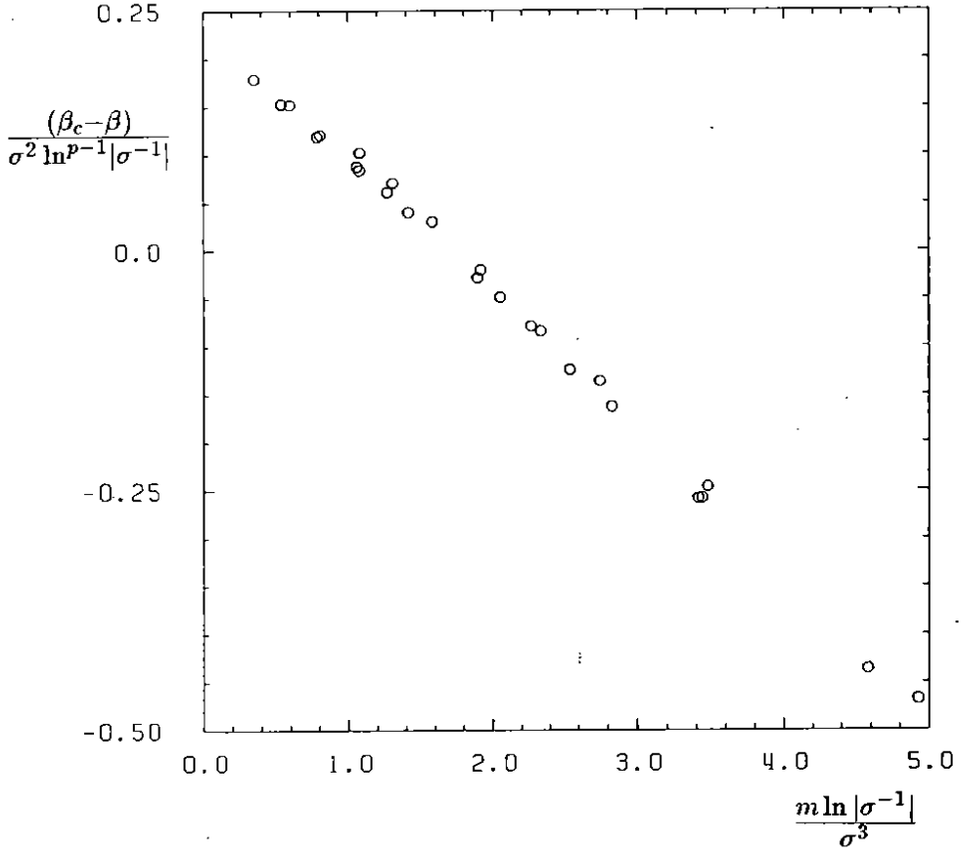

Figure 2

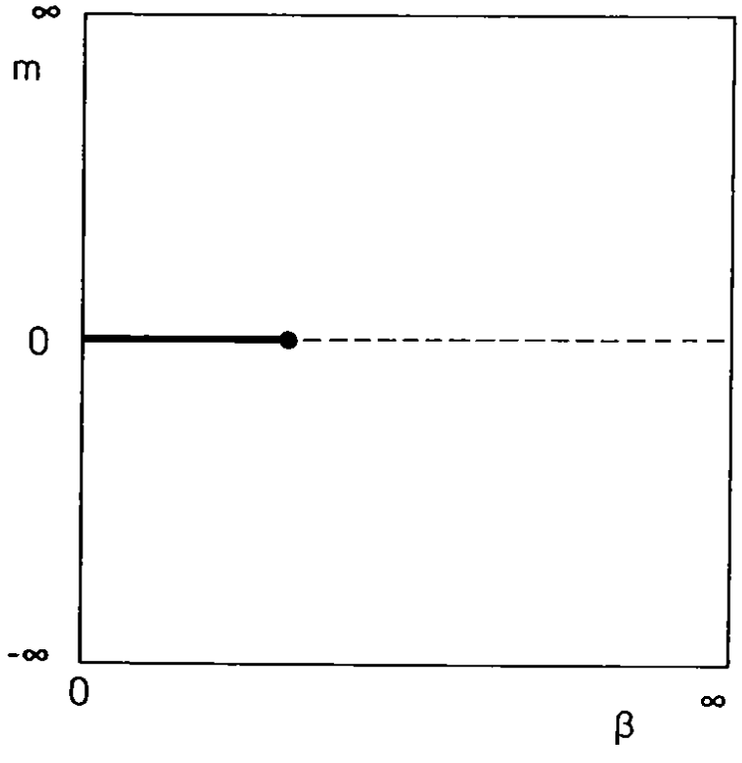

Figure 3

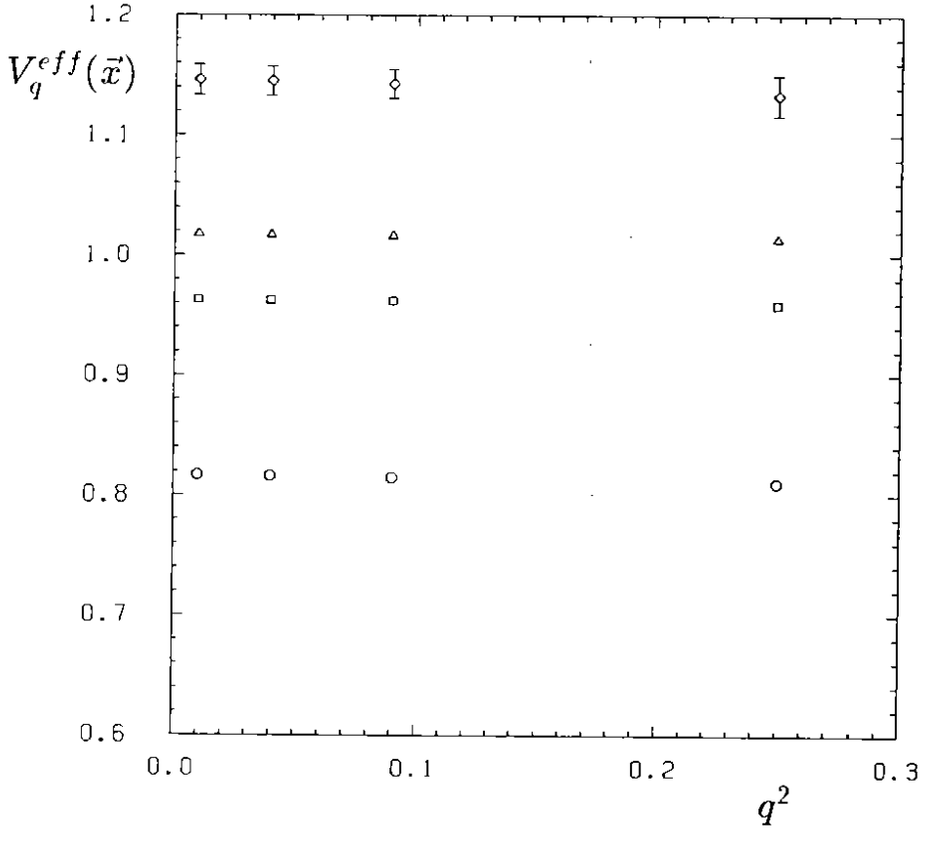

Figure 4

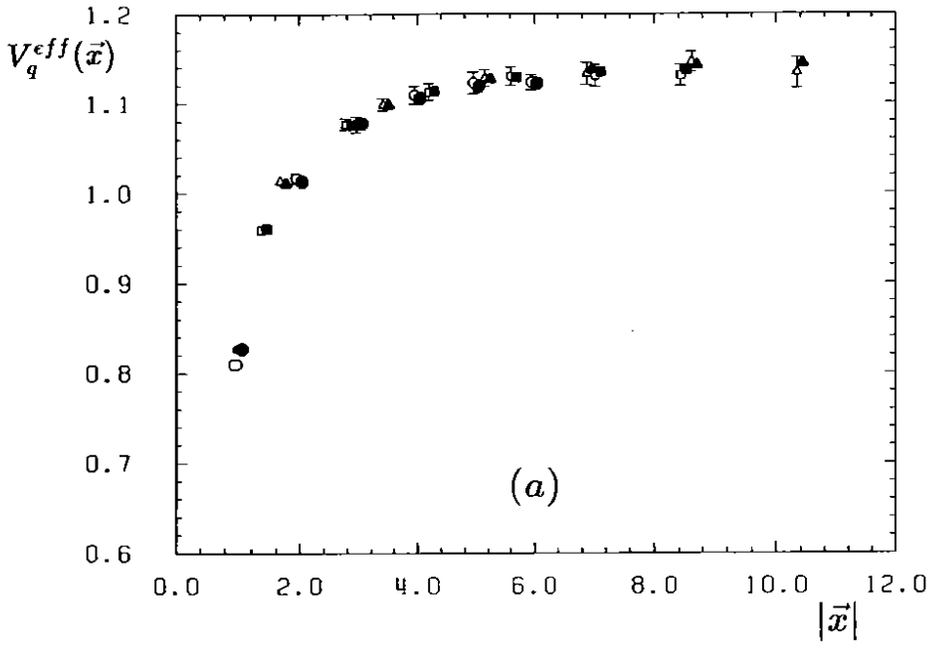

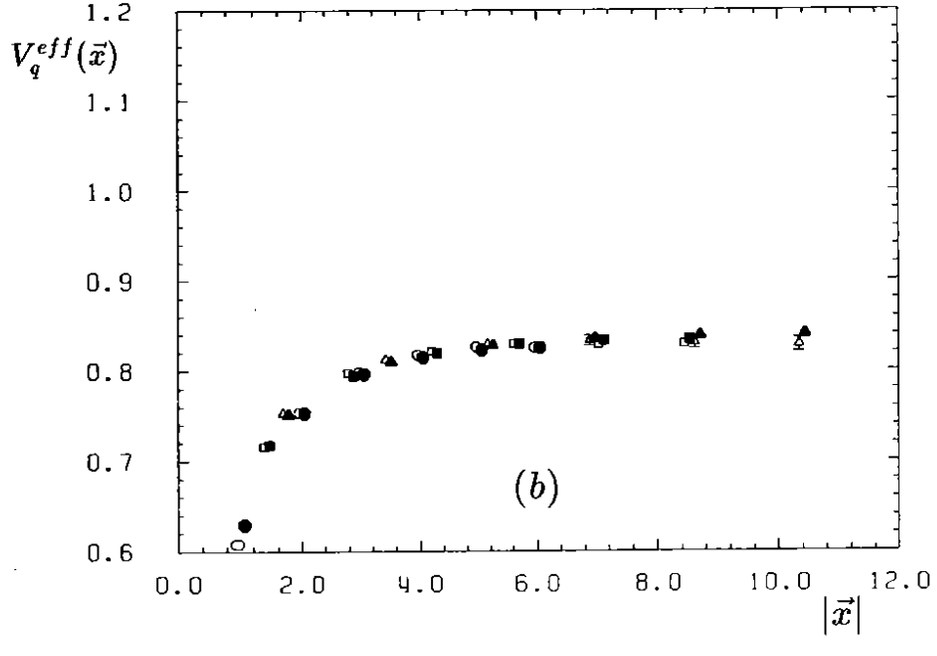

Figure 5

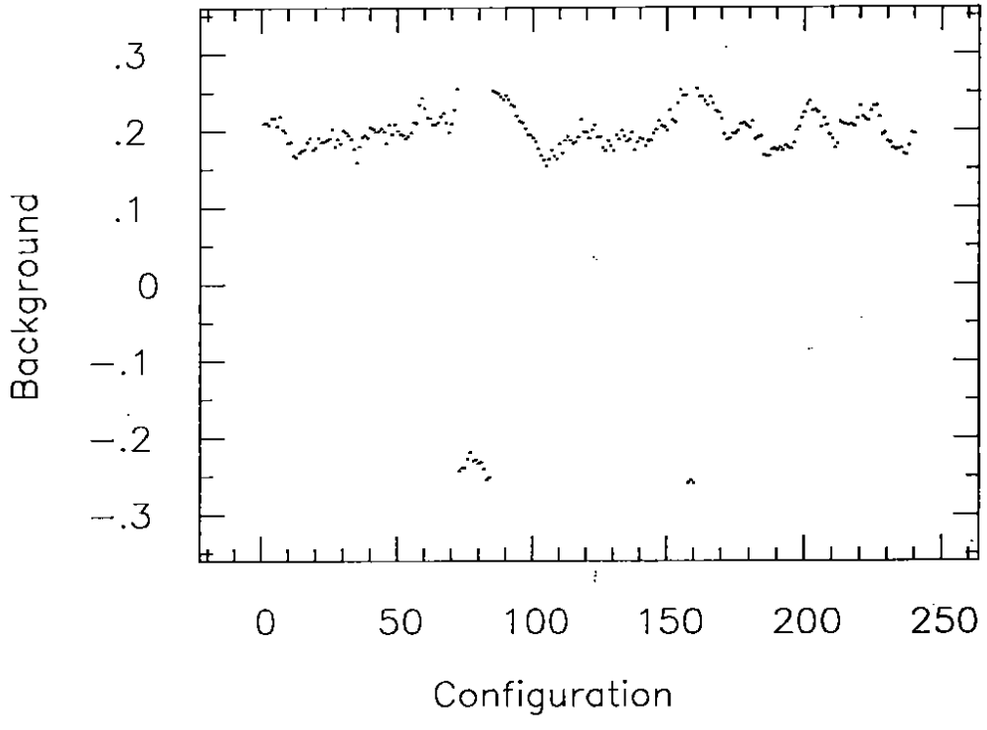

Figure 6

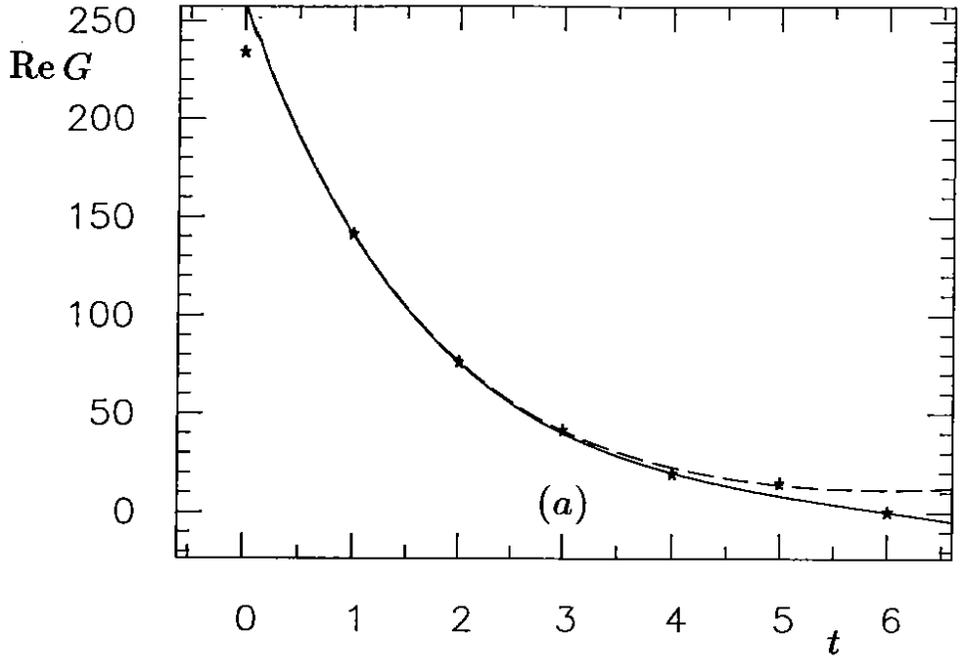

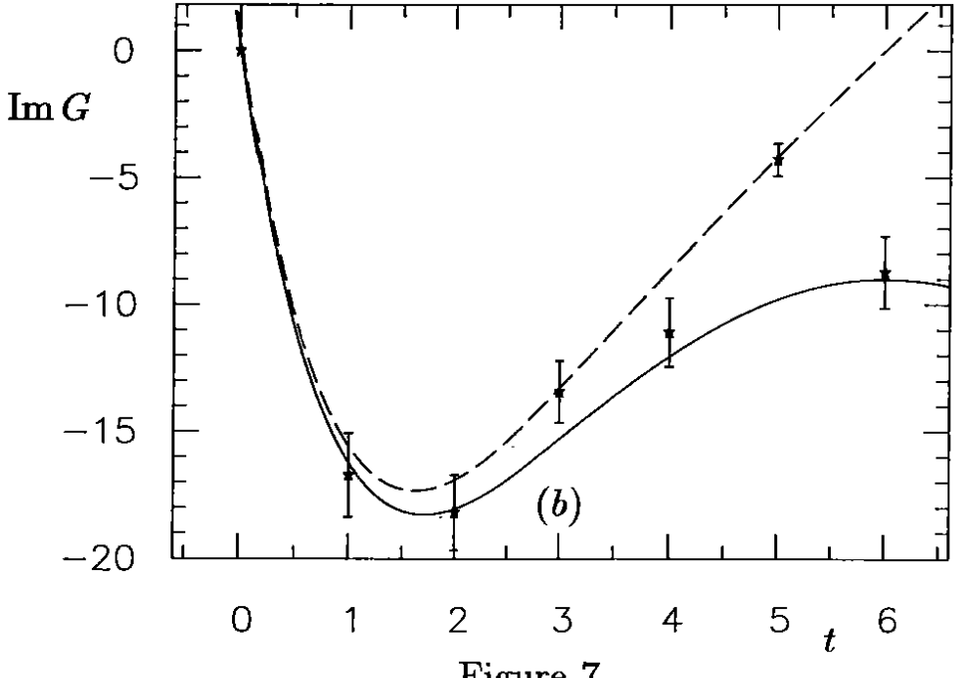

Figure 7

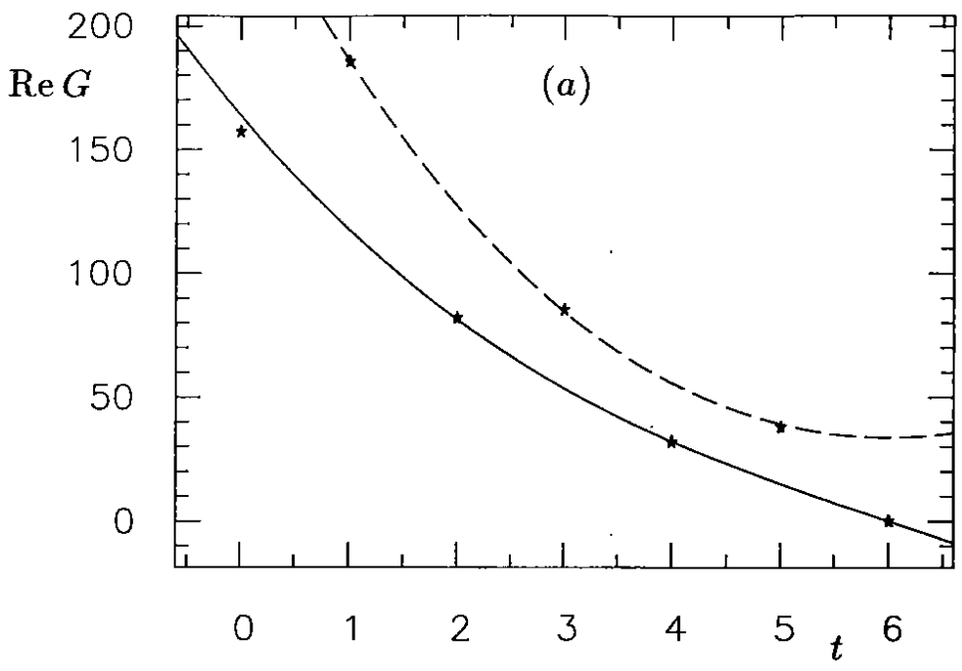

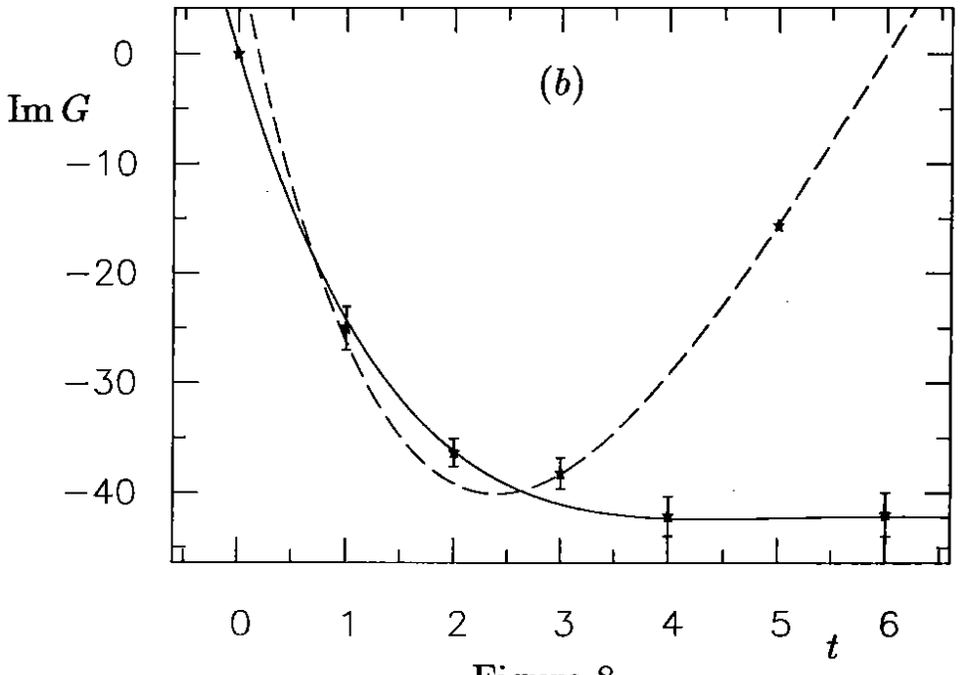

Figure 8

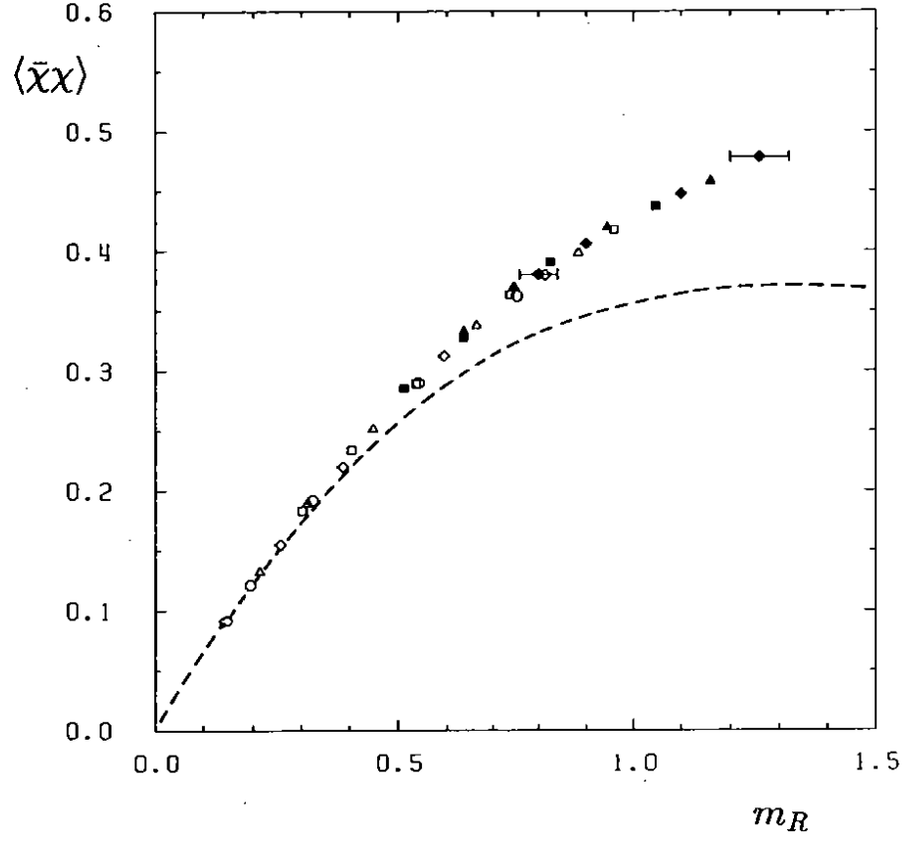

Figure 9

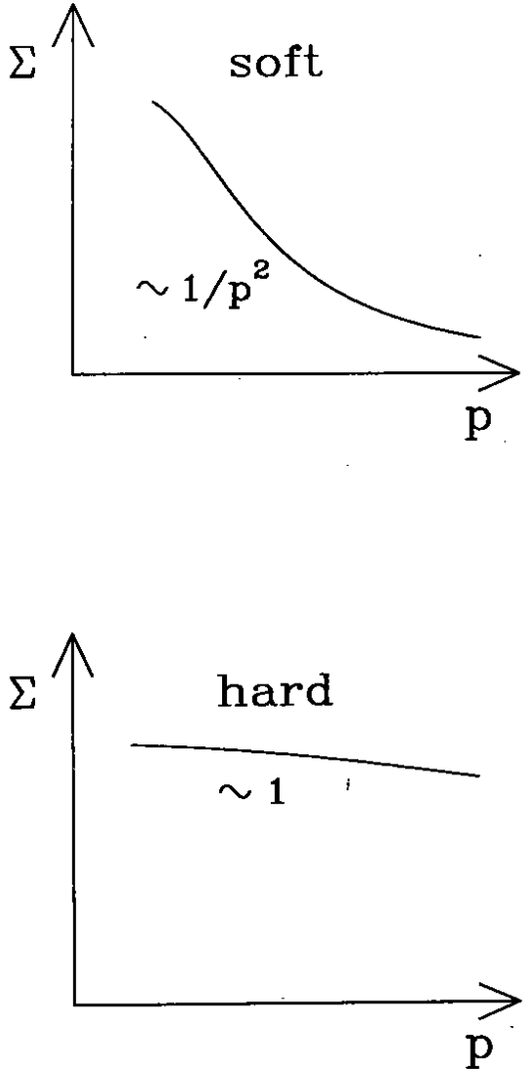

Figure 10

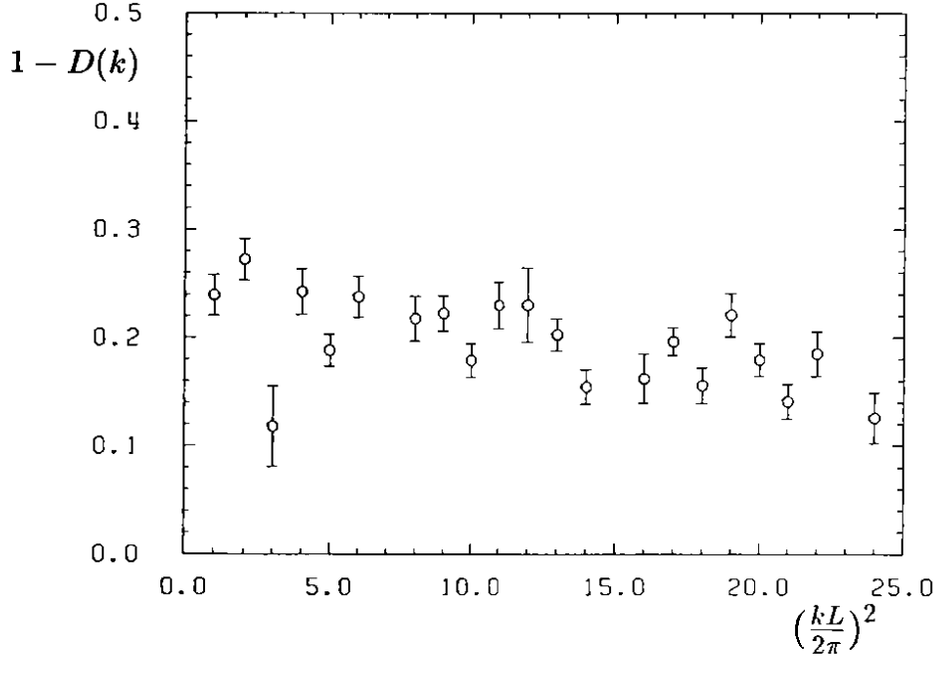

Figure 11

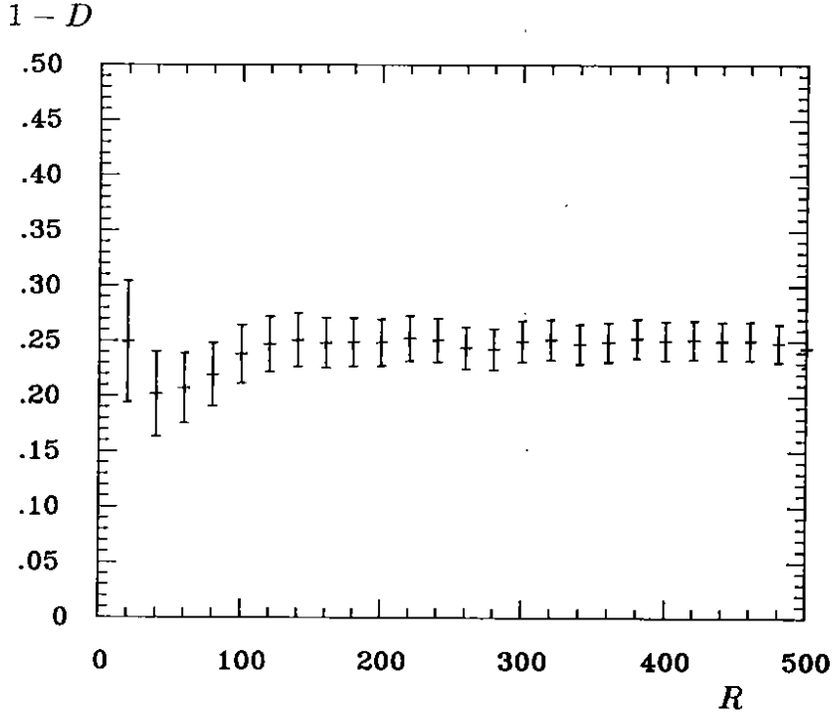

Figure 12

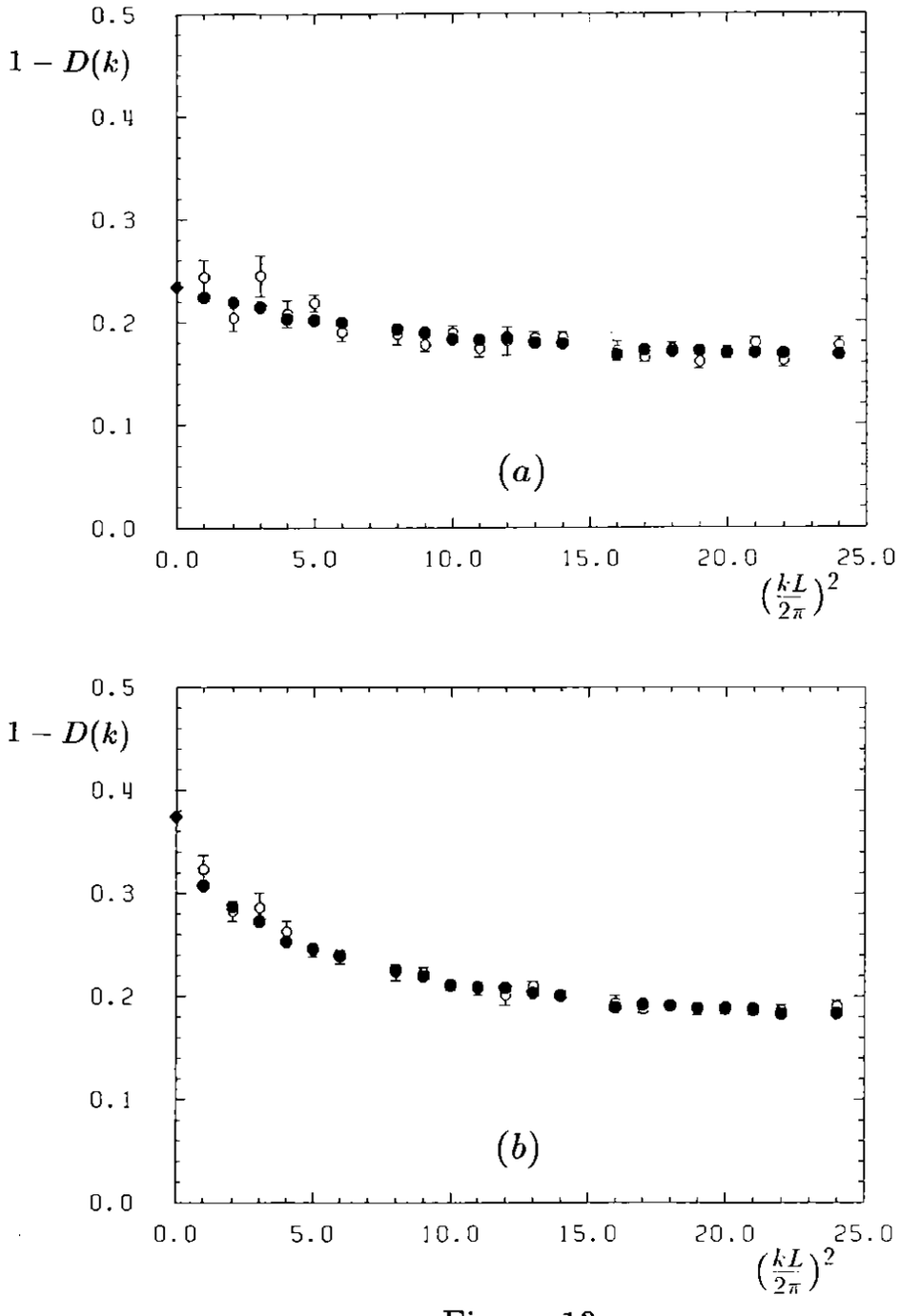

Figure 13

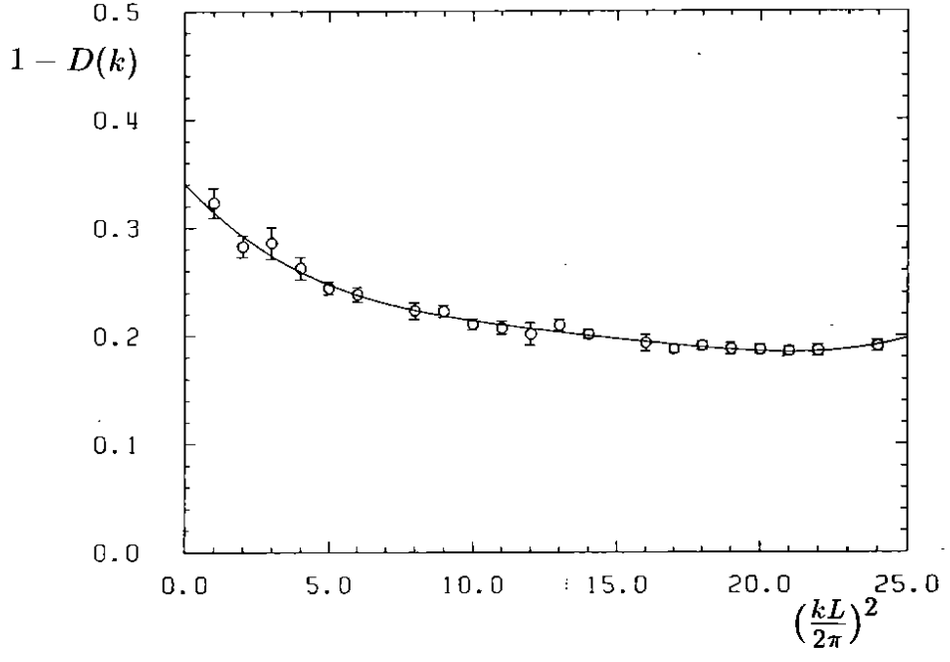

Figure 14

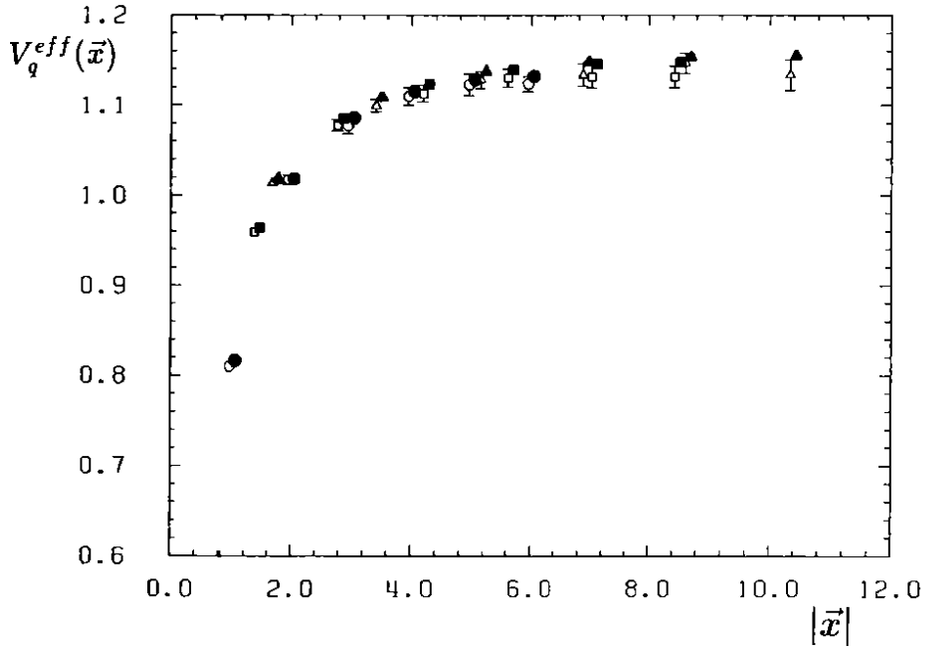

Figure 15

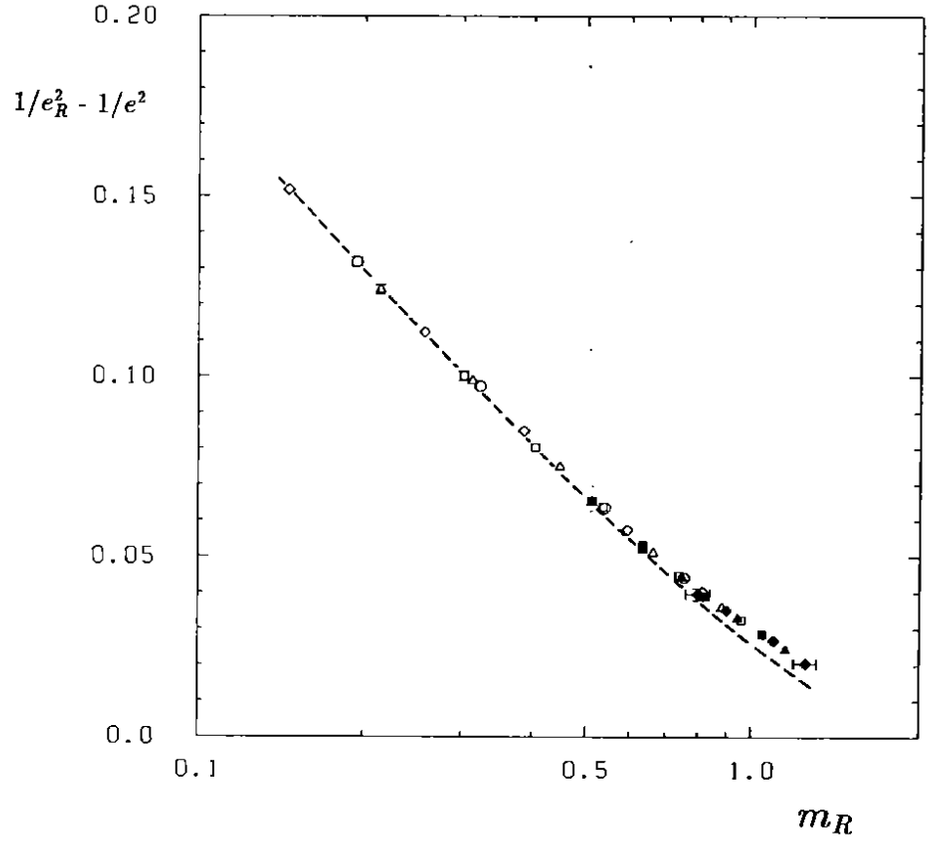

Figure 16

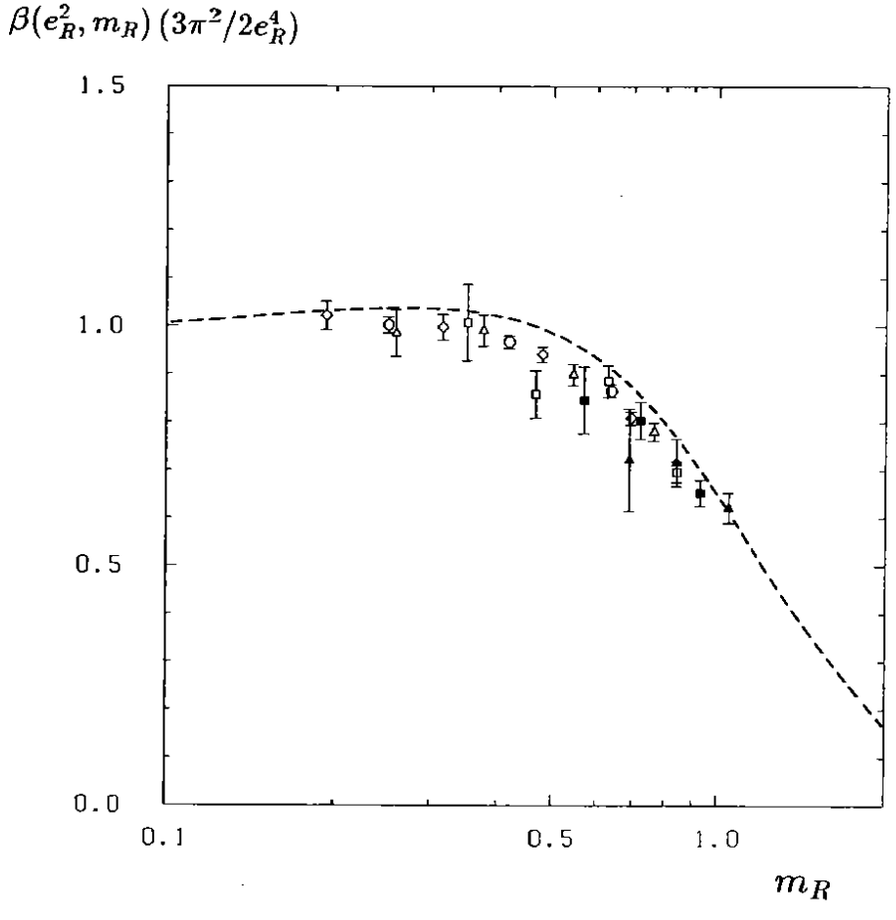

Figure 17

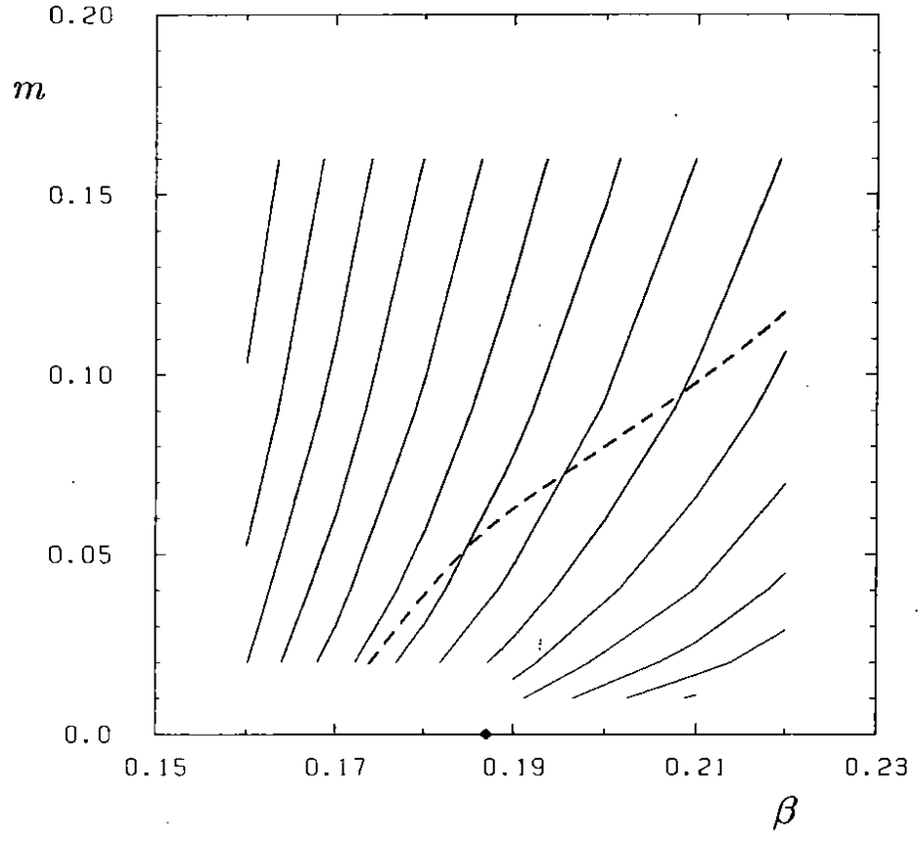

Figure 18

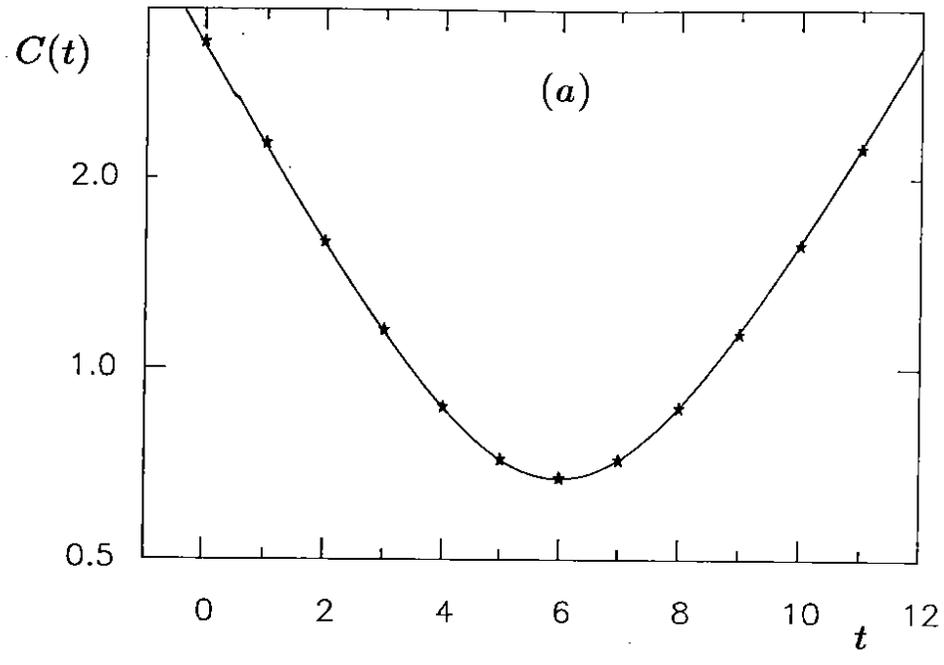

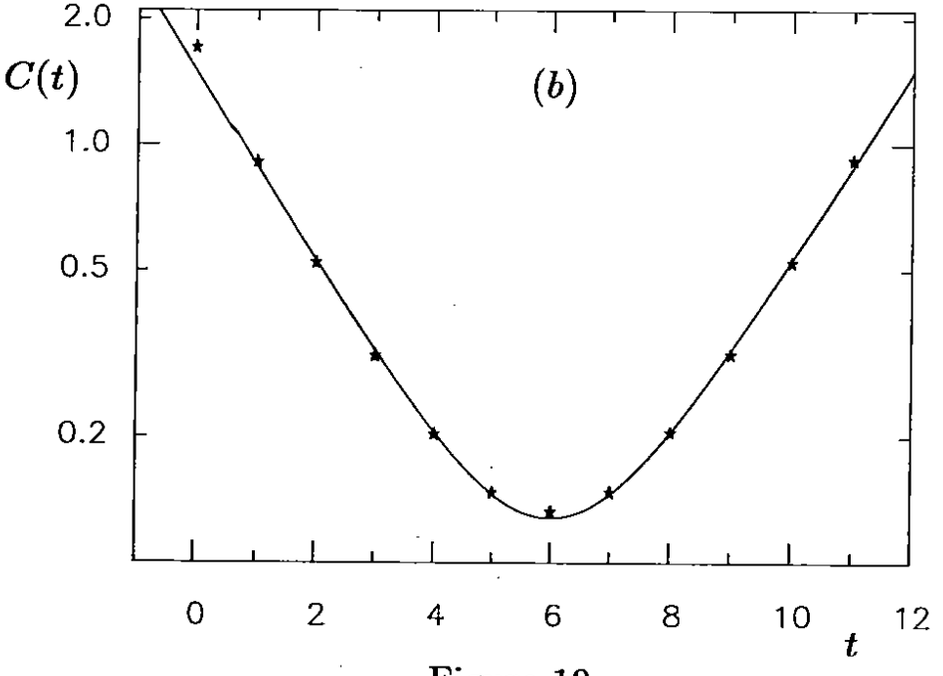

Figure 19

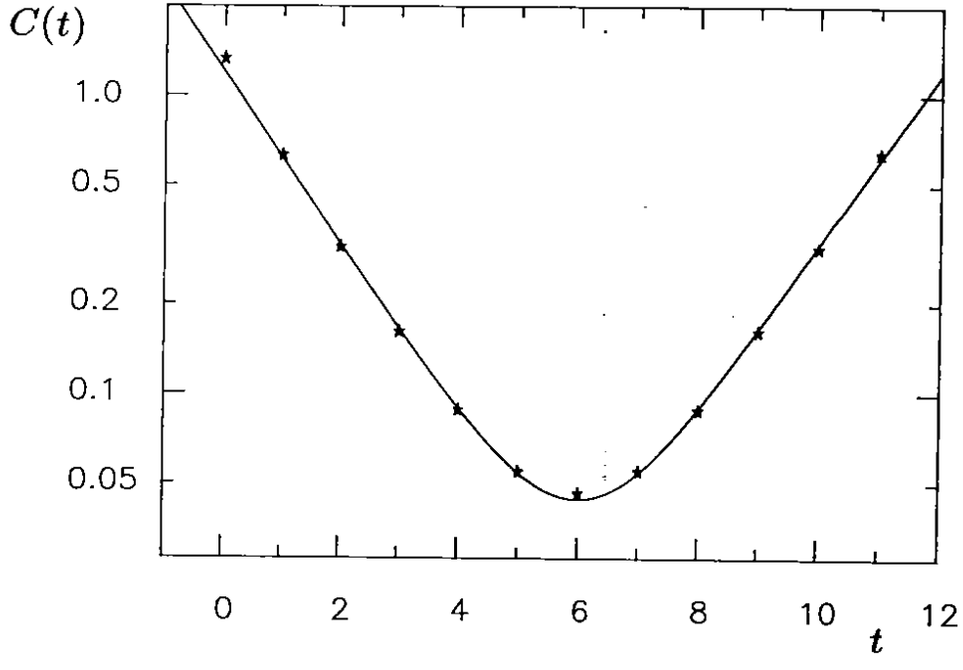

Figure 20

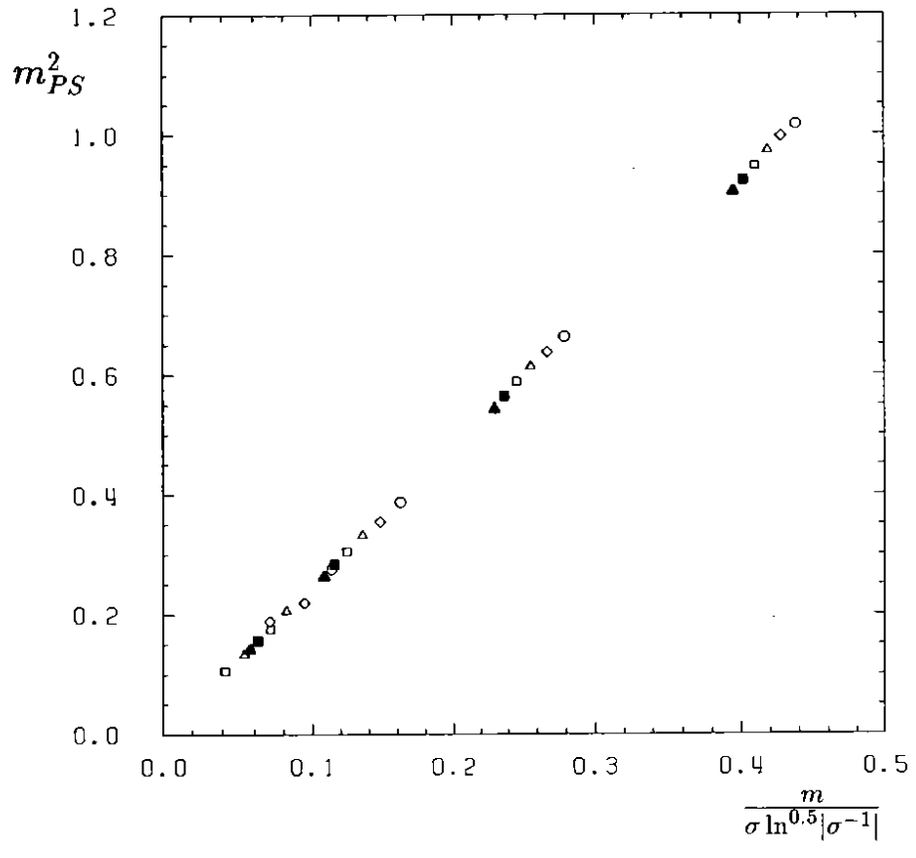

Figure 21

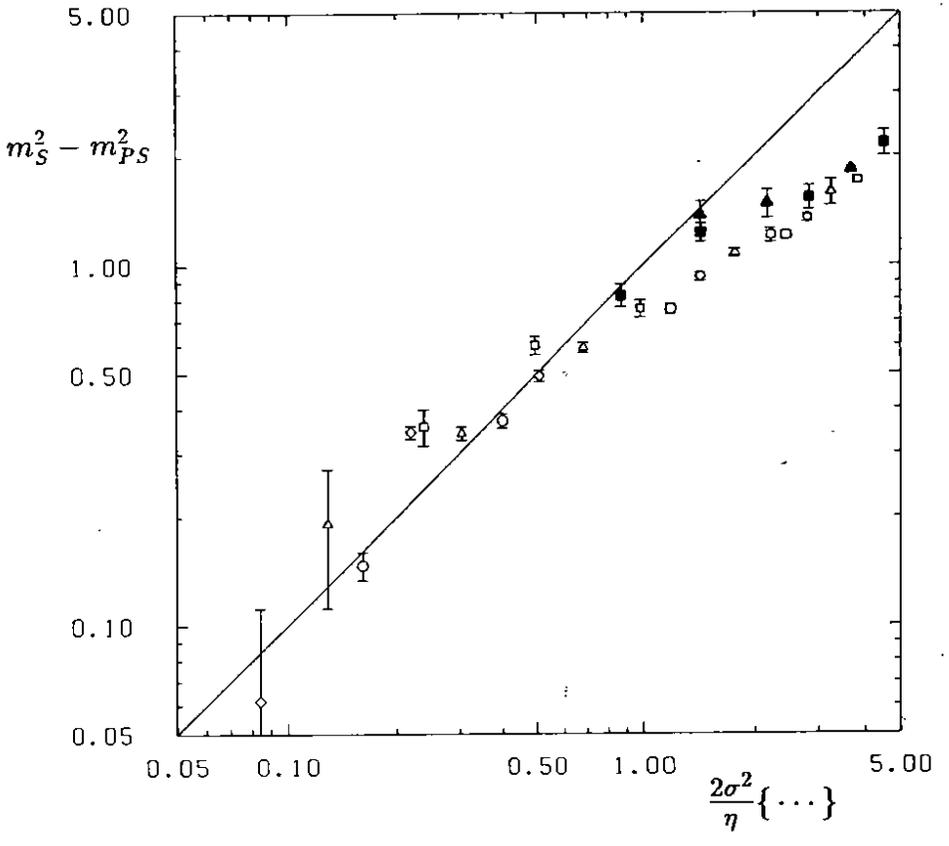

Figure 22

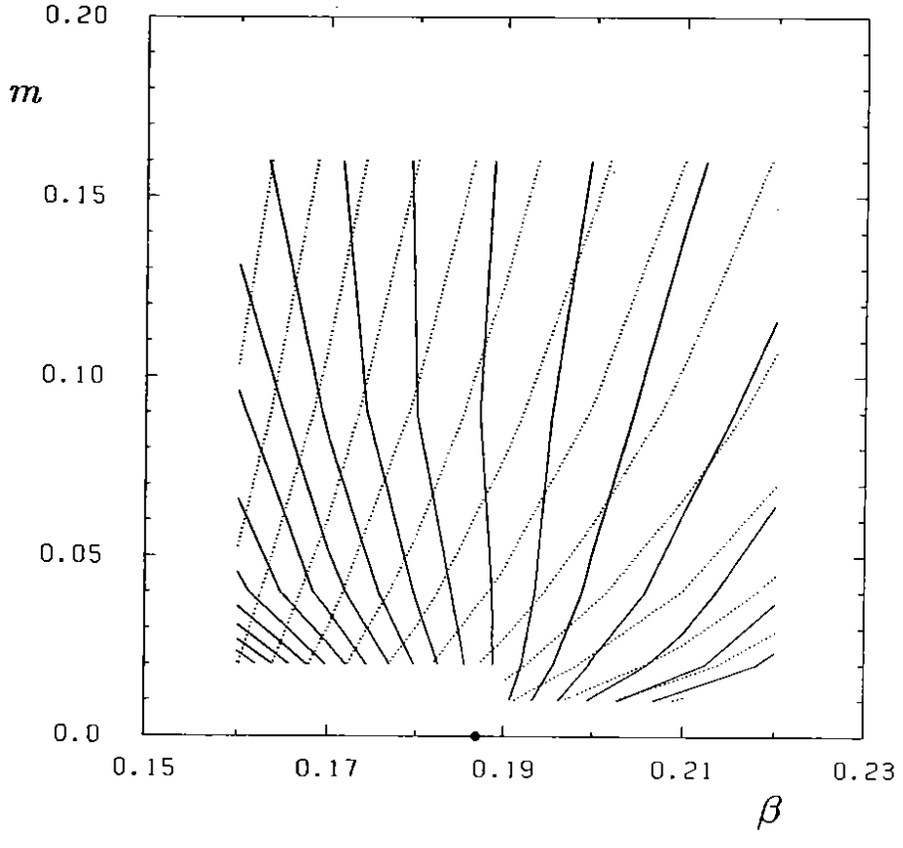

Figure 23

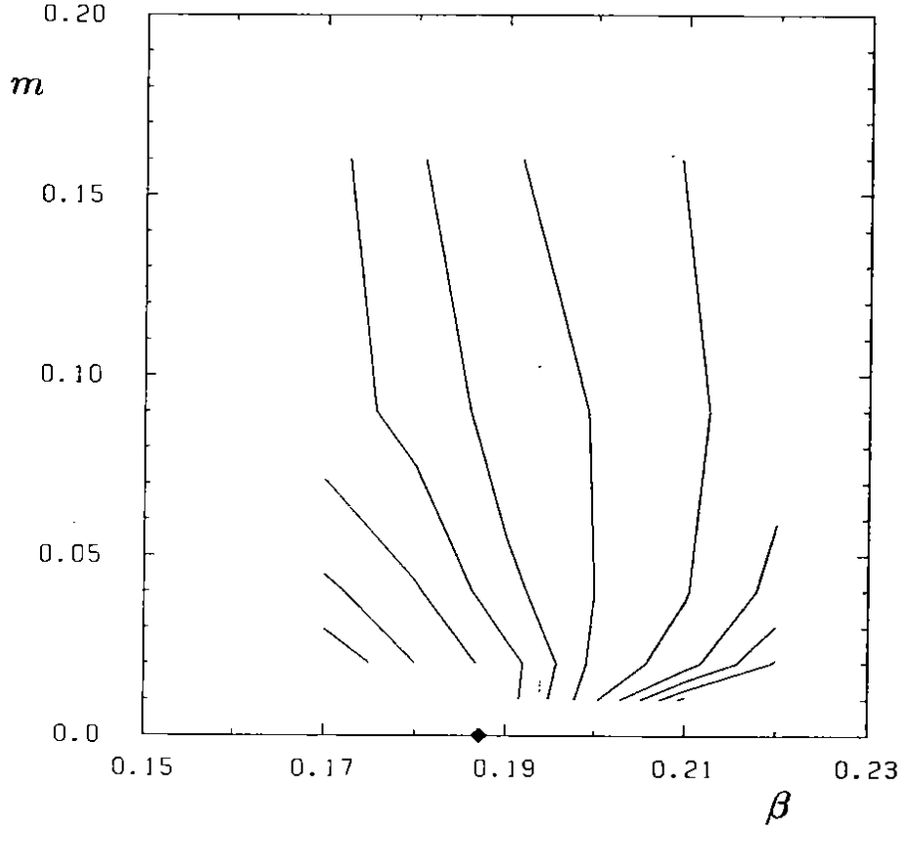

Figure 24

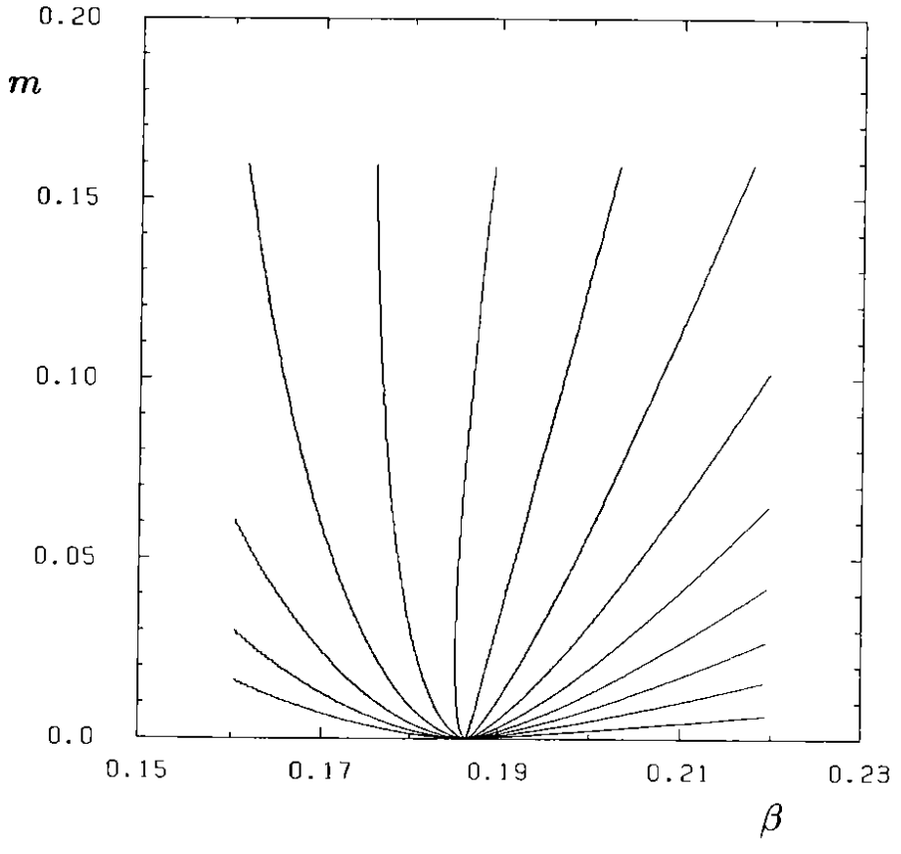

Figure 25

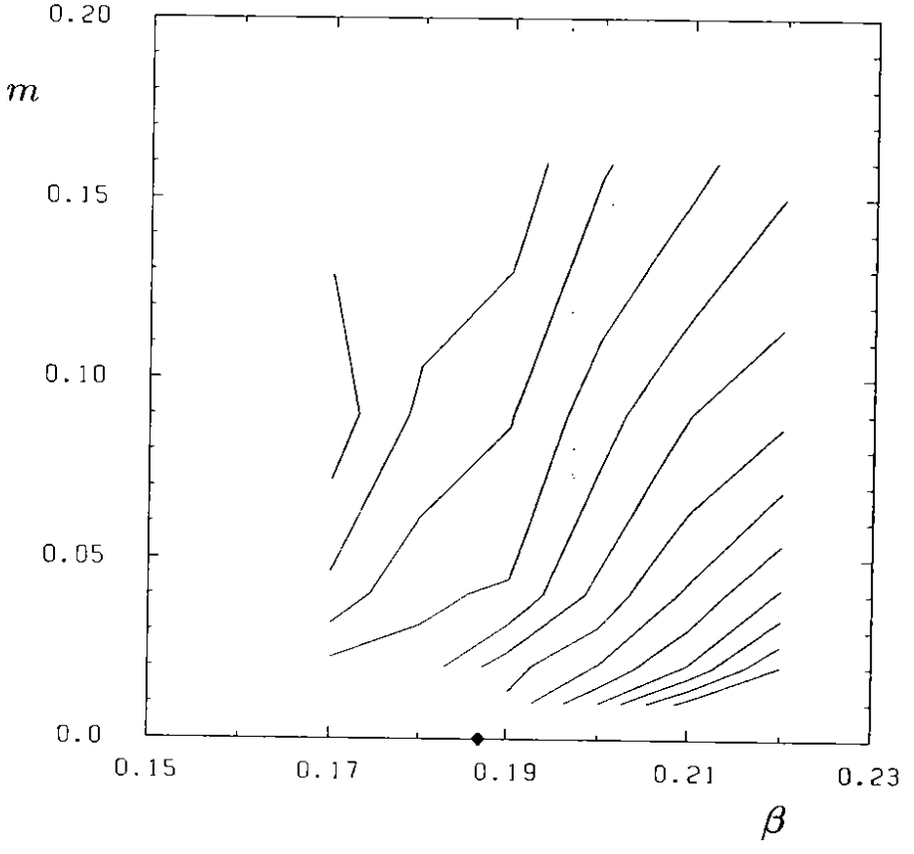

Figure 26